Inhibition of APE1/Ref-1 Redox Signaling Alleviates Intestinal Dysfunction and Damage to Myenteric Neurons in a Mouse Model of Spontaneous Chronic Colitis

Lauren Sahakian,[*] Rhiannon T. Filippone,[*] Rhian Stavely, PhD,[,†] Ainsley M. Robinson, PhD,[*] Xu Sean Yan, PhD,[*] Raquel Abalo, PhD,[‡,§] Rajaraman Eri, PhD,[¶] Joel C. Bornstein, PhD,[‖] Mark R. Kelley, PhD,[**] and Kulmira Nurgali, PhD[*,††,‡‡]*

Background: Inflammatory bowel disease (IBD) associates with damage to the enteric nervous system (ENS), leading to gastrointestinal (GI) dysfunction. Oxidative stress is important for the pathophysiology of inflammation-induced enteric neuropathy and GI dysfunction. Apurinic/apyrimidinic endonuclease 1/redox factor-1 (APE1/Ref-1) is a dual functioning protein that is an essential regulator of the cellular response to oxidative stress. In this study, we aimed to determine whether an APE1/Ref-1 redox domain inhibitor, APX3330, alleviates inflammation-induced oxidative stress that leads to enteric neuropathy in the Winnie murine model of spontaneous chronic colitis.

Methods: Winnie mice received APX3330 or vehicle via intraperitoneal injections over 2 weeks and were compared with C57BL/6 controls. In vivo disease activity and GI transit were evaluated. Ex vivo experiments were performed to assess functional parameters of colonic motility, immune cell infiltration, and changes to the ENS.

Results: Targeting APE1/Ref-1 redox activity with APX3330 improved disease severity, reduced immune cell infiltration, restored GI function ,and provided neuroprotective effects to the enteric nervous system. Inhibition of APE1/Ref-1 redox signaling leading to reduced mitochondrial superoxide production, oxidative DNA damage, and translocation of high mobility group box 1 protein (HMGB1) was involved in neuroprotective effects of APX3330 in enteric neurons.

Conclusions: This study is the first to investigate inhibition of APE1/Ref-1's redox activity via APX3330 in an animal model of chronic intestinal inflammation. Inhibition of the redox function of APE1/Ref-1 is a novel strategy that might lead to a possible application of APX3330 for the treatment of IBD.

Key Words: APE1/Ref-1, APX3330, enteric nervous system, chronic intestinal inflammation, IBD, oxidative stress, DNA damage

INTRODUCTION

Inflammatory bowel disease (IBD) is defined by chronic, recurrent inflammation of the gastrointestinal (GI) tract, characterized by periods of remission and relapses. It is estimated that more than 5 million people globally suffer from IBD.[1] Inflammatory bowel disease encompasses 2 major chronic idiopathic conditions, ulcerative colitis (UC) and Crohn's disease (CD). Ulcerative colitis is confined to the rectum and colon, where it is characterized by mucosal and submucosal ulcerations. In comparison, CD is transmural and displays skip lesions throughout the GI tract, resulting in strictures or fistulas.[2] Inflammatory bowel disease is a complex, multifactorial disorder, and the exact cause is ambiguous. Current treatments are limited by their

Received for publications February 19, 2020; Editorial Decision June 3, 2020.

From the *Institute for Health and Sport, Victoria University; Western Centre for Health, Research and Education, Sunshine Hospital, Melbourne, Victoria, Australia; [†]Department of Pediatric Surgery, Pediatric Surgery Research Laboratories, Massachusetts General Hospital, Harvard Medical School, Boston, MA, USA; [‡]Área de Farmacología y Nutrición y Unidad Asociada al Instituto de Química Médica (IQM) del Consejo Superior de Investigaciones Científicas (CSIC), Universidad Rey Juan Carlos (URJC), Alcorcón, Madrid, Spain; [§]High Performance Research Group in Physiopathology and Pharmacology of the Digestive System at URJC, Alcorcón, Madrid, Spain; [¶]University of Tasmania, School of Health Sciences, Launceston, Tasmania, Australia; [‖]Department of Physiology, Melbourne University, Melbourne, Australia; **Indiana University Simon Comprehensive Cancer Center, Departments of Pediatrics, Biochemistry & Molecular Biology and Pharmacology & Toxicology, Program in Pediatric Molecular Oncology & Experimental Therapeutics, Herman B Wells Center for Pediatric Research, Indiana University School of Medicine Indianapolis, USA; [††]Department of Medicine Western Health, Faculty of Medicine, Dentistry and Health Sciences, The University of Melbourne, Melbourne, Victoria, Australia; [‡‡]Regenerative Medicine and Stem Cells Program, Australian Institute of Musculoskeletal Science (AIMSS), Melbourne, Victoria, Australia

Author Contribution: LS contributed to conception and design, collection, analysis and interpretation of data, and manuscript writing. RTF, RS, and AMR contributed to collection and interpretation of data and manuscript revision. XSY contributed to interpretation of data and manuscript revision. RA, JCB, and MRK contributed to interpretation of data and critical revision of the manuscript. RE contributed to interpretation of data and manuscript revision. KN contributed to conception and design, interpretation of data, manuscript writing, financial support, and project administration. All authors approved the final version of the manuscript.

Conflicts of Interest: The authors declare no conflict of interest.

Supported by: This work was supported by the Institute for Health and Sport, Victoria University. MRK was supported by grants from the National Institute of Health CA167291, CA205166, CA231267, HL140961, and DOD grant W81XWH1910217; he is also supported by the Riley Children's Foundation and the Tom Wood Lexus Foundation.

Address correspondence to: Kulmira Nurgali, Level 4, Research Labs, Western Centre for Health Research & Education, Sunshine Hospital, 176 Furlong Road, St Albans, 3021, VIC, Australia. E-mail: kulmira.nurgali@vu.edu.au.

doi: 10.1093/ibd/izaa161
Published online 3 July 2020

inefficacy and toxic side effects. Most present treatments focus on reducing clinical symptoms and do not exploit the pathogenic mechanisms of the disease; therefore, targeting pathophysiological mechanisms including enteric neuropathy may lead to more effective treatments.

The enteric nervous system (ENS) consists of networks of intrinsic neurons embedded in the wall of the GI tract and controls GI functions with little assistance from the central nervous system.[3] Damage to the ENS is associated with GI dysfunction.[4, 5] The ENS has a vital role in GI immunity, as interactions between enteric neurons and immune cells are important in both normal and pathological conditions.[6] Intestinal inflammation-induced ENS damage associates with a compromised GI antioxidant capacity.[7]

Investigating oxidative stress in inflammatory conditions will provide insight into the pathogenesis of IBD and help to develop new therapies. Exposure of enteric neurons to oxidative stress results in disruption of physiological functions.[8] Colon biopsies from IBD patients have shown increased levels of nitric oxide (NO) and oxidative stress–induced DNA damage measured with a specific marker, 8-hydroxydeoxyguanosine (8-OHdG) .[9, 10]

Apurinic/apyrimidinic endonuclease 1/redox factor-1 (APE1/Ref-1) is a vital dual functioning protein that regulates the cellular response to oxidative stress and acts as a DNA repair protein.[11, 12] The redox active domain of APE1/Ref-1 regulates cellular stress responses, angiogenesis, inflammation, and proliferation.[13, 14] In contrast, its endonuclease repair domain associates with DNA repair.[11, 15–17] Multiple inflammatory conditions produce oxidative stress, resulting in altered APE1/Ref-1 responses; without interception by redox activation, cell apoptosis and carcinogenesis are likely.[18] Previous studies have demonstrated increased APE1/Ref-1 redox activity in tissues removed from IBD patients with active inflammation, indicating underlying oxidative stress within the GI tract.[19, 20] In addition, increased expression of APE1/Ref-1 was observed in colon sections from rats with dextran sodium sulfate (DSS)-induced colitis, which has been associated with an enhanced pro-inflammatory response.[21] Thus, APE1/Ref-1 is involved in the pathophysiology of GI inflammation. Furthermore, APE1/Ref-1 endonuclease activity protects dorsal root ganglion (DRG) neurons from inflammation and chemotherapy-induced oxidative stress and DNA damage.[22, 23]

In this study, we investigated the APE1/Ref-1 redox domain inhibitor, APX3330, as a potential therapeutic agent for treatment of chronic colitis and inflammation-induced enteric neuropathy using the Winnie murine model of spontaneous chronic colitis. In Winnie mice, spontaneous colitis develops from a primary intestinal epithelial defect conferred by a mutation in the *Muc2* mucin gene, leading to intestinal inflammation at 5 to 6 weeks of age and progressing to severe colitis by the age of 12 to 16 weeks. This model closely represents pathophysiological mechanisms and clinical manifestations of human IBD.[24–27]

METHODS

Animals

Male and female Winnie mice (12 w.o; 20–30 g; n = 24) were obtained from the Victoria University Werribee Animal Facility (Melbourne, Australia). Male and female C57BL/6 mice (12 w.o; 20–30 g; n = 12) were obtained from the Animal Resources Centre (Perth, Australia) and were used as controls. All mice were acclimatized for 3 days before receiving their allocated treatments. All mice were housed at the Western Centre for Health, Research, and Education (Melbourne, Victoria, Australia) in a temperature-controlled environment at 22°C with a 12-hour day/night cycle. All animals had free access to food and water. All experimental procedures in this study were conducted in agreement with the Australian National Health and Medical Research Council (NHMRC) guidelines and under animal ethics AEETH 13/001 and AEC 17/016 approved by Victorian University Animal Experimentation Ethic Committee (AEEC).

Administration of APX3330

Winnie mice were randomly divided into 2 groups: APX3330-treated and sham-treated. Winnie APX3330-treated mice received APX3330 (Kelley Laboratory, Indianapolis, IN, USA) at a dose of 25 mg/kg via daily injections dissolved in cremophor (2%; Sigma-Aldrich): ethanol (2%) in sterile water (96%; 30G needle, max volume 200 µL). The dose of APX3330, route of administration, and vehicle solution were based on previous studies in mice.[28, 29] Mice received the treatment over 2 weeks, twice daily with a 12-hour interval. Winnie sham-treated mice received the vehicle daily injections of cremophor (2%; Sigma-Aldrich): ethanol (2%) in sterile water (96%; 30G needle, max volume 200 µL) according to the same regimen as the treatment group.

Disease Activity

Disease activity in Winnie mice can be characterized by clinical signs including rectal prolapse, diarrhea, changes in colon length, and body weight.[24–26, 30] Mice were monitored throughout the treatment period for clinical symptoms. Body weights were recorded daily over a 14-day period and expressed as a percentage of change from the body weight at the start of the treatment. Directly after culling on day 15, the whole colon was excised, and the length was measured to assess changes in colon morphology. Fecal water content was assessed by collection of fresh fecal samples at day 14 before culling for ex vivo motility experiments. Fecal samples were

collected by placing each mouse in a separate sterile cage without bedding until the expulsion of the fecal mass. The samples were immediately weighed to record the wet weight then placed in an oven at +60°C for 24 hours. Dry weight was recorded, and the difference between the wet and dry weight (water content) was calculated as a percentage of the wet weight.

Assessment of Intestinal Inflammation

Measurement of fecal lipocalin (Lcn)-2 was used as a noninvasive detection of anti-inflammatory efficacy of APX3330 treatment.[31] Fecal samples collected on day 14 from C57BL/6 control, *Winnie* sham-treated and *Winnie* APX3330-treated mice were reconstituted in PBS-0.1% Tween 20 (100 mg/mL) to form a homogenous fecal suspension. This was centrifuged for 10 minutes at 12,000 RPM at 4°C. Lcn-2 levels were estimated in the fecal pellet supernatants using Mouse NGAL ELISA Kit Lcn-2 (Abcam 199083). All samples were run in duplicate for statistical value. A microplate reader capable of measuring absorbance at 450 nm, with the correction wavelength set at 540 nm, was used to detect Lcn-2 protein (pg/mL) in the fecal pellet supernatant.

Gastrointestinal Transit

GI transit was measured via a noninvasive radiological method in C57BL/6 control mice and APX3330-treated and sham-treated Winnie mice after completion of treatment on day 14 as previously described.[31] Briefly, C57BL/6 control, Winnie sham-treated, and Winnie APX3330-treated mice received barium sulfate as contrast (2.5 mg/mL; maximum volume of 200 µL; X-OPAQUE-HD) via oral gavage. Sequential x-rays were taken using HiRay Plus Porta610HF x-ray apparatus (JOC Corp, Kanagawa, Japan; 50 kV, 0.3 mAs, exposure time 60 ms) immediately postbarium sulfate administration (0 min) and then every 10 minutes for the first hour, followed by every 20 minutes until expulsion of the first pellet with barium sulphate or a maximum of 4 hours. Images were processed through Fujifilm FCR Capsule XL11 and analyzed on eFilm 4.2.0 software. Parameters of GI transit were measured by time (mins) to determine contrast passing through whole GI tract (whole transit time), stomach to cecum (gastro-cecal transit time; GCTT), cecum retention time, and leaving cecum to anus (colonic transit time; CTT). The C57BL/6 control, APX3330-treated, and sham-treated Winnie mice were culled on the following day (day 15), and tissues were collected for ex-vivo studies.

Organ Bath Experiments for Isolated Colonic Motility

Whole colons were removed from C57BL/6 control, Winnie sham-treated, and Winnie APX3330-treated mice in oxygenated physiological saline, and ex vivo organ-bath colonic motility experiments were performed as described previously.[31–33] Briefly, colons were positioned horizontally and cannulated at the oral and anal ends in an organ bath superfused with Kreb's solution (composition in mM: NaCL 118, KCl 4.6, $CaCl_2$ 3.5, $MgSO_4$ 1.2, NAH_2PO_4 1, $NaHCO_3$ 25 and d-Glucose 11; bubbled with 95% O_2 and 5% CO_2) while maintained at a constant temperature of 37°C. The oral cannula was connected to a reservoir containing Kreb's solution that was adjusted to maintain intraluminal pressure (0 to +2 cm H_2O). The anal end was coupled to an outflow tube with a maximum backpressure of 2 cm H_2O. Colonic contractile activity was recorded by a video camera positioned above the organ bath. Tissues were left to equilibrate at constant intraluminal pressure for 30 minutes followed by 2 sequential 20-minute video recordings of colonic contractile activity. Videos were transposed into spatiotemporal maps with Scribble v2.0 software and were analyzed using MATLAB v2017a software to assess parameters of colonic motility.

Tissue Collections

Distal colon tissues were harvested in oxygenated physiological saline, flushed clear of fecal content, and cut along the mesenteric border. Tissues were pinned down with the mucosal side up in a Sylgard-lined Petri dish and fixed with Zamboni's fixative (2% formaldehyde containing 0.2% picric acid) overnight at 4°C. The fixative was removed by a series of washes (3 × 10 minutes) with dimethyl sulfoxide (DMSO; Sigma-Aldrich, Sydney, Australia) followed by three 10-minute washes with phosphate buffered saline (PBS). For cross-sections, distal colon tissues were pinned and fixed as previously described without stretching, then covered by 50:50 optimum cutting temperature (OCT) compound (Tissue Tek, CA, USA) and frozen in liquid nitrogen–cooled isopentane and OCT and stored at –80°C until cryo-sectioned (20 µm) onto glass slides. For wholemount longitudinal muscle with attached myenteric plexus (LMMP) preparations, distal colon segments were stretched to maximum capacity without tearing, fixed, and washed as previously described. To expose the myenteric plexus, the mucosa, submucosa, and circular muscle layers were removed before immunohistochemical labeling.

Immunohistochemistry and Histology

Immunohistochemistry was performed as previously described.[26] Cross-sections and wholemount LMMP preparations were incubated for 1 hour at room temperature in 10% normalized donkey serum (Merck Millipore, Australia). Preparations were then washed (2 × 5 mins) with PBS and incubated with primary antisera (Table 1) overnight at room temperature in an enclosed moist environment. Cross-sections and LMMP preparations were washed with 1x PBS (3 × 10 minute) and incubated with fluorophore-conjugated secondary antisera Alexa Fluor 488, 594, or 647 of the respective antihost species

(1:200; Jackson Immunoresearch, West Grove, PA, USA) for 2 hours at room temperature. All specimens were stained with 4', 6'-diamindino-2-pheylindole dihydrochloride (DAPI) to label cell nuclei. Tissues were given 3 × 10 minutes final washes in PBS, mounted on glass slides, and cover slipped with fluorescent mounting medium (DAKO, Australia).

Tissues for histology were cryo-sectioned at 10 µm, cleared and rehydrated in graded ethanol concentration. For standard hematoxylin and eosin staining (H&E), sections were immersed in histolene (3 × 4 minutes), 100% ethanol (2 minutes), 95% ethanol (2 minutes), 70% ethanol (2 minutes), rinsed in tap water (30 seconds), then in hematoxylin (Sigma-Aldrich; 1 minute), rinsed in tap water, immersed in Scott's tap water (1 minute) and eosin (Sigma-Aldrich; 5 minutes), rinsed in tap water, immersed in 100% ethanol (2 × 1 minute) and histolene (4 minutes), and finally mounted on glass slides with DPX mounting media. A histological grading system was used to evaluate gross morphological damage from the following parameters: aberrant crypt architecture (score range, 0–3), changes to crypt length (0–3), crypt abscesses (0–3), leukocyte infiltration (0–3), epithelial damage (0–3), and ulceration (0–3); there was an average of 3 areas of 500 µm^2 per section. Slides were imaged using an Olympus BX53 microscope (Olympus Imaging, Sydney, Australia). All slides were coded, and analysis was performed blindly.

Imaging and Quantitative Analysis

Triple-labeled specimens were visualized and imaged via confocal microscopy (Nikon Eclipse Ti multichannel confocal laser scanning system, Nikon, Japan) using combinations of FITC, Alexa 594, and Alexa 647 filters (495 nm, 559 nm, or 640.4 nm excitation wavelength respectively). Images (1062 × 1062 pixels) were obtained with 20x (dry) or 40x and 60x (oil immersion) lenses. Immunoreactivity for CD45, β-Tubulin, and APE1/Ref-1 was analyzed in cross-sections and quantified as a percentage of the area with specific fluorescence relative to the total 2 mm^2 area of colonic mucosa. Images of 3 colon sections from each tissue sample were captured with a 20x objective to quantify the average area of fluorescence. Immunoreactivity for glial fibrillary acidic protein (GFAP), MitoSOX, and APE1/Ref-1 in LMMP preparations was analyzed in 5 randomly chosen myenteric ganglia. Fluorescence was measured as a percentage relative to the ganglion area, using ImageJ software (NIH, Bethesda, MD, USA). All images for CD45, β-Tubulin, APE1/Ref-1, GFAP, and MitoSOX were acquired with equal acquisition and exposure time conditions, calibrated to standard minimum baseline fluorescence, and converted to binary for analysis of the number of fluorescent pixels per image.[31, 32] Data were normalized and presented as percentage due to the variability in different ganglia and colon sizes between groups. The number of myenteric neurons were counted within 10 randomly selected ganglia (expressed as an average number of neurons per ganglion) and within 4 randomly chosen images per preparation at 20x magnification (total area 1 mm^2; expressed as number of neurons per area). The number of neurons with translocation of high mobility group box 1 (HMGB1) from the nuclei to the cytoplasm was quantified with the aid of the nuclei marker DAPI. Longitudinal muscle with attached myenteric plexus preparations were colabeled with MAP2 and 8-OHdG to identify oxidative stress–induced DNA damage within myenteric neurons. The number of myenteric neurons colocalized with 8-OHdG was quantified as a proportion of the total number of neurons within an average of 10 myenteric ganglia. Neurons were counted using the Cell Counter plug-in in ImageJ software. All slides were coded and images were analyzed blindly.

TABLE 1. Primary Antisera Utilized for Immunohistochemistry

Primary Antisera	Target	Host Species	Titration	Specimen	Supplier
Anti-CD45 (ab10558)	Leukocyte Infiltration	Mouse	1:500	Cross-sections	Abcam
Anti-β-tubulin III (ab18207)	Nerve fibers	Rabbit	1:1000	Cross-sections	Abcam
Anti-MAP2 (ab5392)	Neurons	Chicken	1:5000	LMMP	Abcam
Anti-GFAP (ab53554)	Glial Cells	Goat	1:500	LMMP	Abcam
Anti-APE1/Ref-1	APE1 protein	Mouse	1:1000	Cross-sections LMMP	Produced by Mark Kelley's lab
Anti-HMGB1 (ab227168)	Damage-associated molecular protein	Mouse	1:500	LMMP	Abcam
Anti-8-OHdG (ab48508)	DNA Damage	Mouse	1:200	LMMP	Abcam

Superoxide Production in the Myenteric Plexus

MitoSOX Red M36008 (Thermo Fisher Scientific, Scoresby, VIC, Australia) was used to identify mitochondrial-derived production of superoxide in the myenteric ganglia.[32] Briefly, freshly excised preparations of the distal colon from C57BL/6 control, Winnie sham-treated, and Winnie APX3330-treated mice were dissected to expose the myenteric plexus. Samples were incubated with 5μM MitoSOX Red M36008 at 37°C for 40 minutes. Tissues were washed with oxygenated Krebs solution and fixed with Zamboni's fixative for 1 hour followed by PBS washes (3 × 10 minutes). Preparations were mounted on glass slides with DAKO fluorescent mounting medium for imaging. Images were captured as described previously. Images were converted into binary, and fluorescent areas were measured in arbitrary units relative to ganglion area using ImageJ software (NIH).

Statistical Analysis

The data and statistical analysis comply with the recommendations on experimental design and analysis in pharmacology.[34] Data were assessed using 1-way ANOVA with Tukey post hoc tests for multiple group comparison. Analyses were performed using Graph Pad Prism (Graph Pad Software Inc., San Diego, CA, USA). Data are presented as mean ± standard error of the mean (SEM). Value differences were considered statistically significant at $P < 0.05$.

RESULTS

APX3330 Treatment Improved Clinical Symptoms in *Winnie* Mice

C57BL/6 control mice did not display any symptoms of inflammation; the signs of diarrhea, rectal prolapse, and bleeding were absent; all C57BL/6 mice produced firm pellets during the 14-day period. All Winnie mice had chronic diarrhea before start of the treatments. Winnie sham-treated mice had chronic diarrhea throughout the whole treatment period; some mice had rectal prolapse evident as a rectal protrusion with edema and bleeding (Fig. 1A). Winnie APX3330-treated mice that had rectal prolapse at the start of the treatment demonstrated reduced rectal prolapse, edema, and bleeding by day 14 of the treatment regimen (Fig. 1A). Colons were excised, and their length was measured at day 15 (Fig. 1B). Colons from Winnie sham-treated mice had shorter lengths (75.7 ± 3.2 mm, $P < 0.01$, n = 5) than C57BL/6 control mice (90.4 ± 3.8 mm, n = 5) and contained soft fecal masses (Fig. 1B'). The APX3330 treatment did not improve the colon lengths (70.4 ± 1.9 mm, $P < 0.05$, n = 5); however, the presence of hard fecal pellets was prominent similar to C57BL/6 control mice (Fig. 1B-B'). Fecal water content was used as a measure of diarrhea. Fresh fecal pellets were collected on day 14 to assess water content. Winnie sham-treated mice had higher level of fecal water content (83.4 ± 2.7%, $P < 0.0001$, n = 7) than C57BL/6 control mice (57.3 ± 0.6%, n = 7; Fig. 1C). Conversely, feces from Winnie APX3330-treated mice had lower fecal water retention (73.2 ± 2.1%, $P < 0.01$, n = 7) than Winnie sham-treated mice but higher levels than C57BL/6 control mice ($P < 0.0001$; Fig. 1C). Haematoxylin and eosin staining was performed in colon cross-sections to evaluate gross morphological alterations using parameters described in Methods (Fig. 1D). Winnie sham-treated mice attained a higher histological score (8.9 ± 1.4, $P < 0.0001$, n = 5) compared with C57BL/6 control mice (0.5 ± 0.2, n = 5; Fig. 1D'). The APX3330 treatment reduced histological score in Winnie mice (8.9 ± 1.4, $P < 0.001$, n = 5). Body weights of C57BL/6 control, Winnie sham-treated, and Winnie APX3330-treated mice were measured over the 14-day period (Fig. 1E). Winnie sham-treated mice showed progressively decreasing body weight which was significantly different from day 6 until day 14 compared with C57BL/6 control mice (Fig. 1E). Winnie APX3330-treated mice grew slowly but not equally well as control C57BL/6 mice and weighed significantly more (99.8 ± 1.0%, $n = 8$) than Winnie sham-treated mice at day 14 (93.3 ± 1.8%, $P < 0.05$, n = 10; Fig. 1E).

APX3330 Treatment Reduced Inflammation in the Colon

A pan-leukocyte marker anti-CD45 antibody was used in colon cross-sections to investigate whether APX3330 treatment reduced immune cell infiltration in the Winnie mice colons (Fig. 2A). The density of CD45-IR cells quantified as a percentage of the CD45-IR area relative to the total 2 mm^2 area of colonic mucosa was significantly higher in Winnie sham-treated mice (24.9 ± 1.8%, n = 5) than in C57BL/6 control (13.6 ± 0.6%, $P < 0.01$, n = 5) and Winnie APX3330-treated (12.0 ± 1.3%, $P < 0.01$, n = 5) mice (Fig. 2B). Severity of intestinal inflammation was assessed by the presence of rectal prolapse and Lipocalin-2 (Lcn-2) levels in the feces. Lipocalin-2, also known as neutrophil gelatinase-associated lipocalin, is a noninvasive, highly sensitive and specific biomarker for intestinal inflammation.[35] At day 14, Winnie sham-treated mice displayed a higher fecal Lcn-2 level (46 ± 2.4 pg/mL, n = 5) than C57BL/6 control mice (28 ± 2.4 pg/mL, $P < 0.001$, n = 5). Treatment with APX3330 decreased fecal Lcn-2 levels (39 ± 1.8 pg/mL, $P < 0.01$, n = 5), although these were still greater than in C57BL/6 controls (Fig. 2C).

APX3330 Treatment Improved GI Transit in Winnie Mice

The efficacy of APX3330 treatment was assessed on parameters of GI transit and colonic motility. Radiographic images captured movement of the contrast agent barium sulfate from the stomach to the rectum in C57BL/6 control (Fig. 3A), Winnie sham-treated (Fig. 3A') and Winnie APX3330-treated (Fig. 3A'') mice. Total transit time in Winnie sham-treated

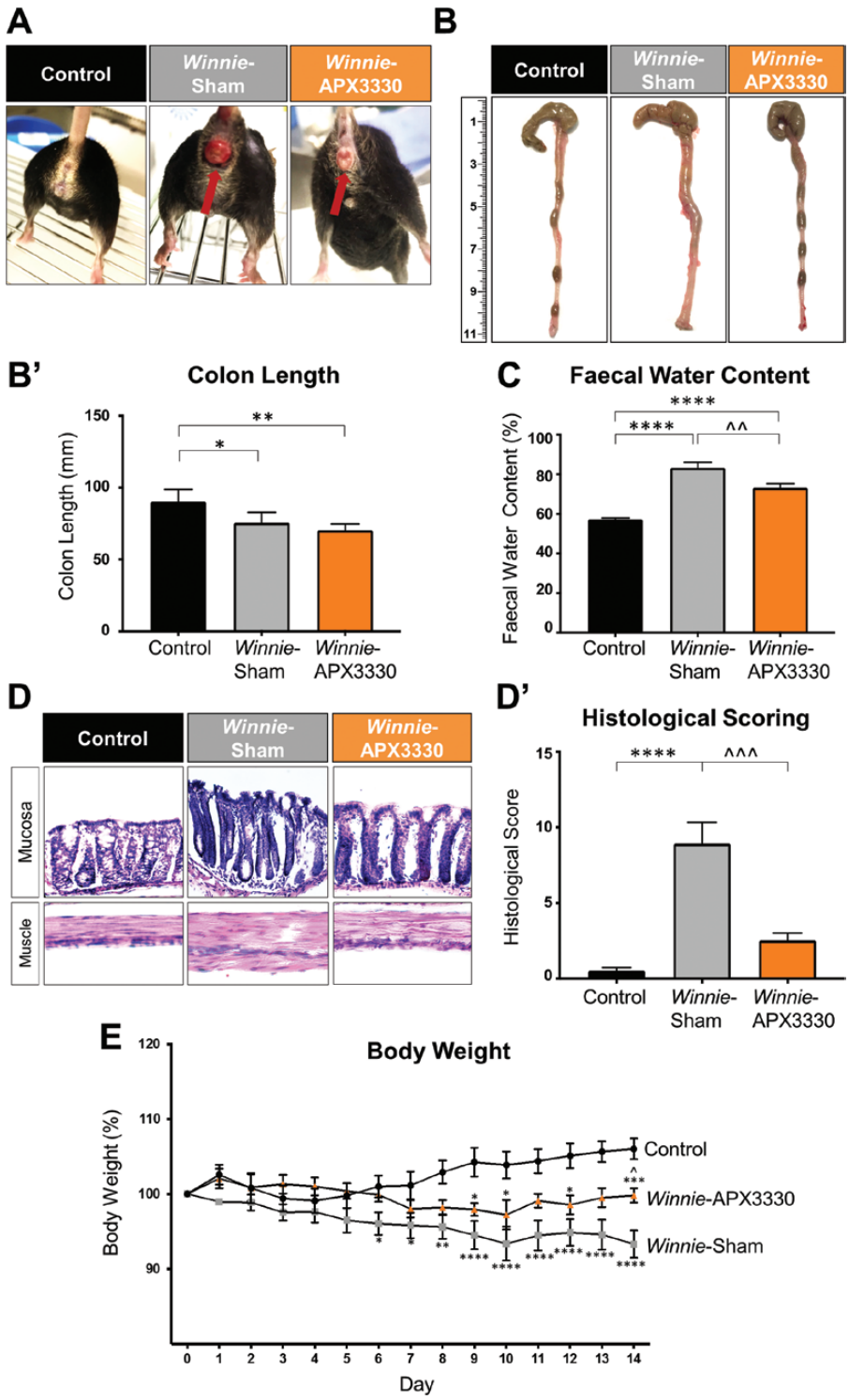

FIGURE 1. The effects of APX3330 treatment on clinical symptoms in *Winnie* mice. A, Images of a C57BL/6 control mouse and a *Winnie* sham-treated mouse with severe intestinal inflammation and rectal prolapse with blood vessel proliferation and edema before and after 14 days of APX3330 treatment. **B, B'.** Colons from C57BL/6 control, *Winnie* sham-treated and *Winnie* APX3330-treated mice were excised and their length (mm) measured at day 15 ($n = 5$/group). C, Fecal water content (the difference between the wet and dry weight) was calculated as a percent of the wet weight of fresh fecal pellets measured at day 14 of treatment (n = 7/group). **D, D'.** Gross morphology of the distal colon was assessed by H&E staining and histological scoring was quantified in distal colon cross-sections from C57BL/6 control, *Winnie* sham-treated and *Winnie* APX3330-treated mice ($n = 5$/group). E, Body weight loss or gain in C57BL/6 control ($n = 10$), *Winnie* sham-treated ($n = 10$) and *Winnie* APX3330-treated ($n = 8$) mice over the 14-day period. Data expressed as mean ± SEM, $^{*}P < 0.05$, $^{**}P < 0.01$, $^{***}P < 0.001$, $^{****}P < 0.0001$ compared with C57BL/6 control mice; $^{\wedge}P < 0.05$, $^{\wedge\wedge}P < 0.01$ compared with *Winnie* sham-treated mice.

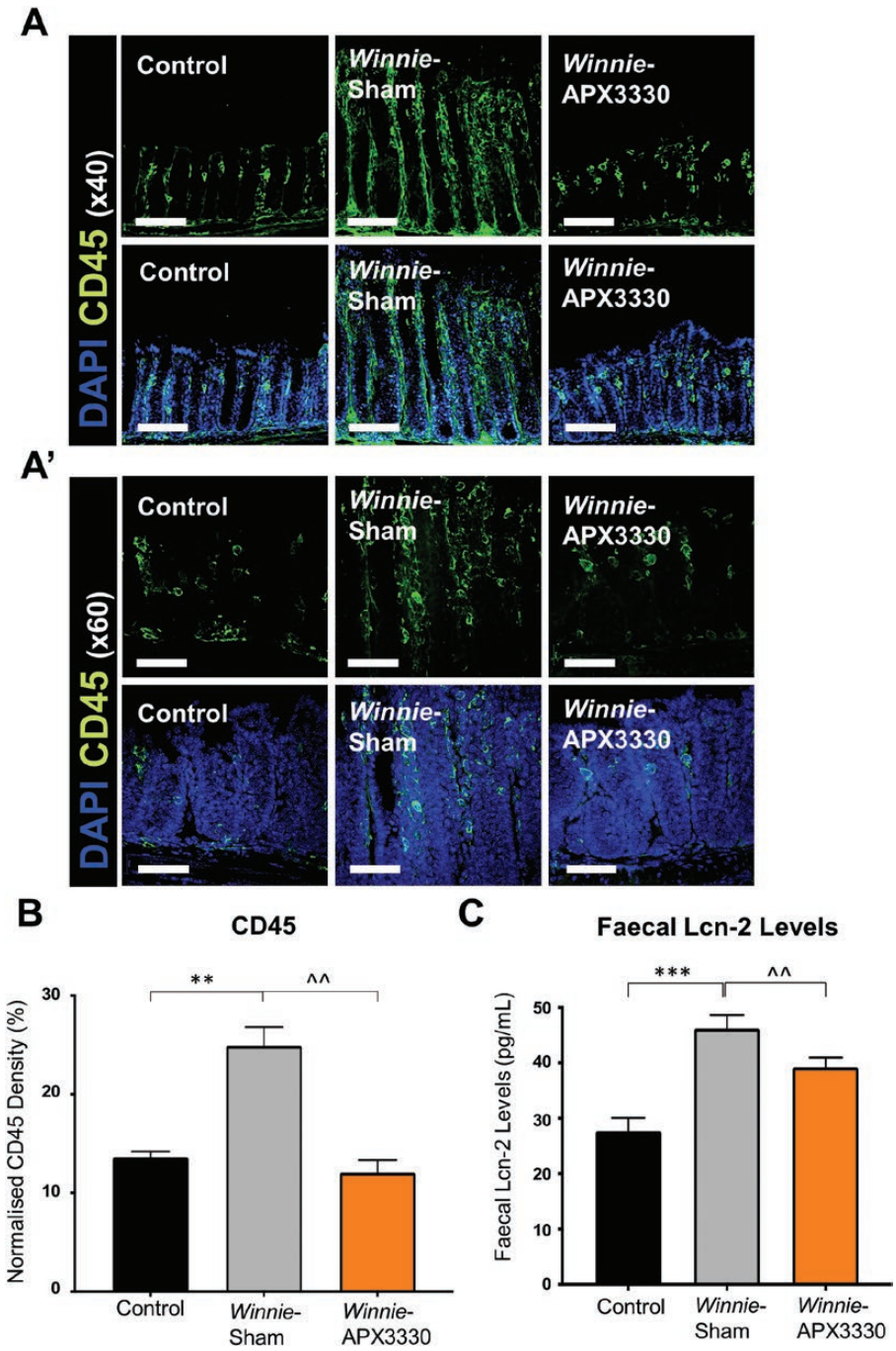

FIGURE 2. The anti-inflammatory effects of APX3330 treatment in the colon of Winnie mice. A, and A') CD45+ leukocytes were labeled using a leukocyte marker anti-CD45+ (green) antibody in the colon cross-sections. Mucosal epithelial cells are labeled with nuclei marker DAPI (blue; A: scale bar = 50 µm, 40x magnification; A': scale bar = 30 µm, 60x magnification). B, Density of CD45+-IR cells normalized to the width of the colon sections in C57BL/6 control, Winnie sham-treated and Winnie APX3330-treated mice (n = 5/group). C, Lipocalin-2 (Lcn-2) levels in fecal pellets were quantified from C57BL/6 control, Winnie sham-treated, and Winnie APX3330-treated mice (n = 5/group). Data expressed as mean ± SEM, $^{**}P < 0.01$, $^{***}P < 0.001$ compared with C57BL/6 control mice; $^{\wedge\wedge}P < 0.01$ compared with Winnie sham-treated mice.

(232.9 ± 5.7 mins, n = 7) was longer than in C57BL/6 control (174.3 ± 11.1 mins, $P < 0.01$, n = 7) mice. The APX3330 treatment reduced the total transit time in Winnie mice (163.3 ± 18.9 mins, $P < 0.05$, n = 7) to a level comparable with C57BL/6 control mice (Fig. 3B). No significant differences between experimental groups were observed in gastro-cecal transit time (GCTT; Fig. 3C), but other parameters of GI transit were compromised in Winnie sham-treated mice and restored in Winnie APX3330-treated mice. Winnie sham-treated mice had a prolonged contrast retention time in the cecum (165.7 ± 9.7

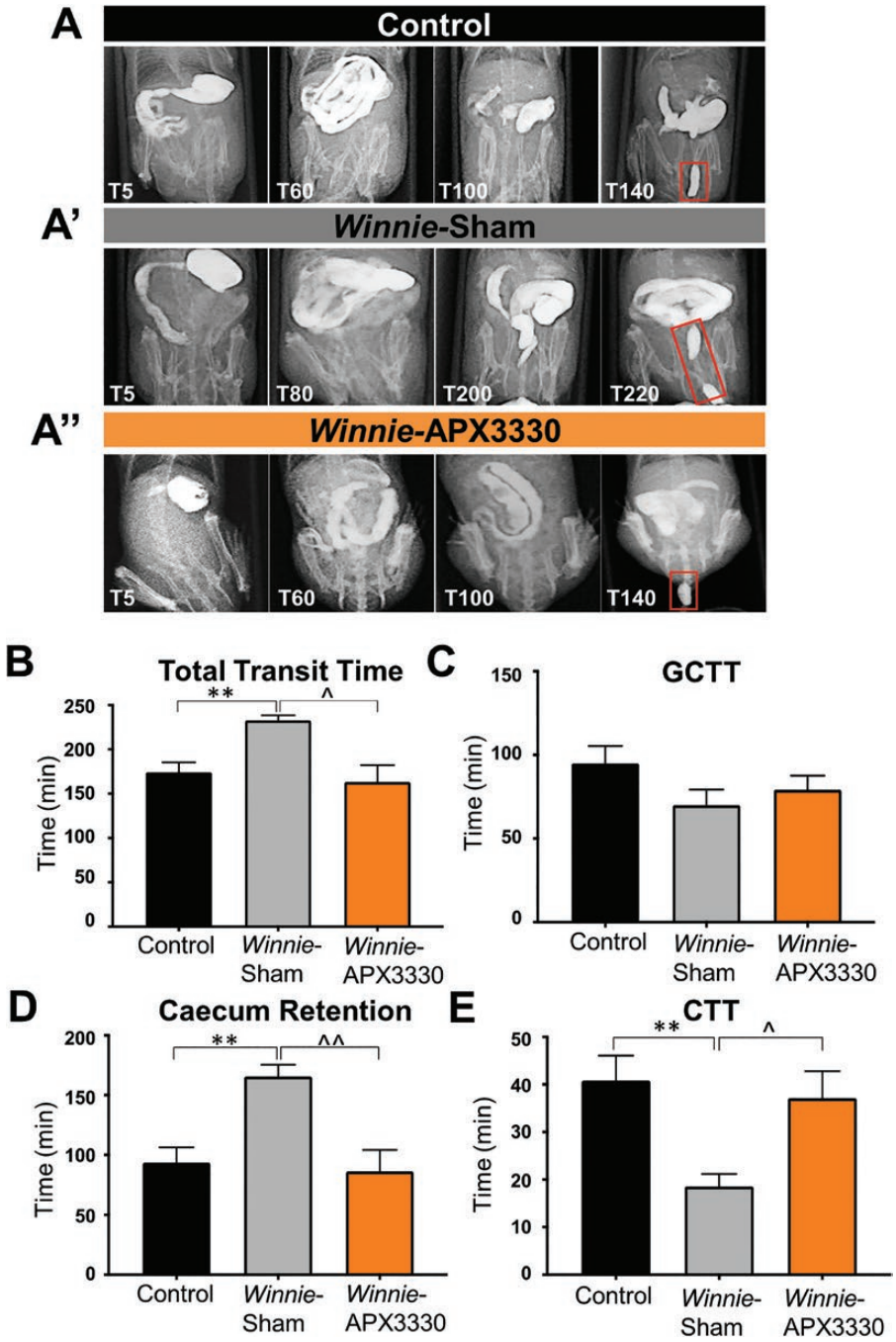

FIGURE 3. The effects of APX3330 treatment on gastrointestinal transit. A, A'') Radiographic images captured movement of the contrast agent and barium sulfate from the stomach to the expulsion of the first pellet (shown in red rectangles) in C57BL/6 control, Winnie sham-treated, and Winnie APX3330-treated mice (n = 7/group). B, Overall gastrointestinal transit time extended in Winnie sham-treated mice and subsided in Winnie APX3330-treated mice. C, Gastro-cecal transit time (GCTT) demonstrated no significant changes between C57BL/6 control, Winnie sham-treated, and Winnie APX3330-treated mice. D, A prolonged cecum retention time was observed in Winnie sham-treated mice and was attenuated in Winnie APX3330-treated mice. E, Colonic transit time (CTT) was accelerated in Winnie sham-treated mice, was comparable with C57BL/6 control mice, and was improved in Winnie APX3330-treated animals. Data expressed as mean ± SEM, $^{**}P < 0.01$ compared with C57BL/6 control mice; $^{\wedge}P < 0.05$, $^{\wedge\wedge}P < 0.01$ compared with Winnie sham-treated mice.

mins, n = 7) compared with C57BL/6 control mice (93.6 ± 12.8 mins, $P < 0.01$, n = 7). But the cecum retention time in Winnie APX3330-treated (86.4 ± 17.8 mins, $P < 0.01$ compared with Winnie sham-treated group, n = 7) was similar to that of C57BL/6 control mice (Fig. 3D). In contrast, colonic transit time was shorter in Winnie sham-treated mice (18.6 ± 2.6 mins,

n = 7) than in C57BL/6 control mice (40.8 ± 5.2 mins, $P < 0.01$, n = 7) but was restored to control levels in Winnie APX3330-treated mice (37.1 ± 5.7 mins, $P < 0.05$ compared with Winnie sham-treated group, $n = 7$; Fig. 3E).

The effects of APX330 treatment on colonic contractile activity was assessed in ex vivo organ bath experiments (Fig. 4). Colonic migrating motor complexes (CMMCs) are identified as contractions initiated from the oral end that propagated toward the anal end for >50% of the colon length.[31, 36] Video recordings were converted into spatiotemporal maps with contractions identified as orange/red lines (Fig. 4A). Overall, the average length of colonic contractions in Winnie sham-treated mice (21.0 ± 2.6%, n = 6) was much shorter than in C57BL/6 control mice (79.9 ± 4.5%, $P < 0.0001$, n = 6). The APX3330 treatment increased the length of colonic contractions (74.3 ± 1.7%, $P < 0.0001$, $n = 6$; Fig. 4B). Lengths of CMMCs in *Winnie* sham-treated (50.2 ± 7.2%, $n = 6$) mice were significantly shorter than in C57BL/6 control mice (68.9 ± 3.7%, $P < 0.05$, $n = 6$; Fig. 4C). *Winnie* APX3330-treated mice had lengths of CMMCs (72.7 ± 0.8%, $P < 0.05$, $n = 6$) similar to those of C57BL/6 control mice (Fig. 4C). CMMCs were significantly faster in *Winnie* sham-treated mice (average

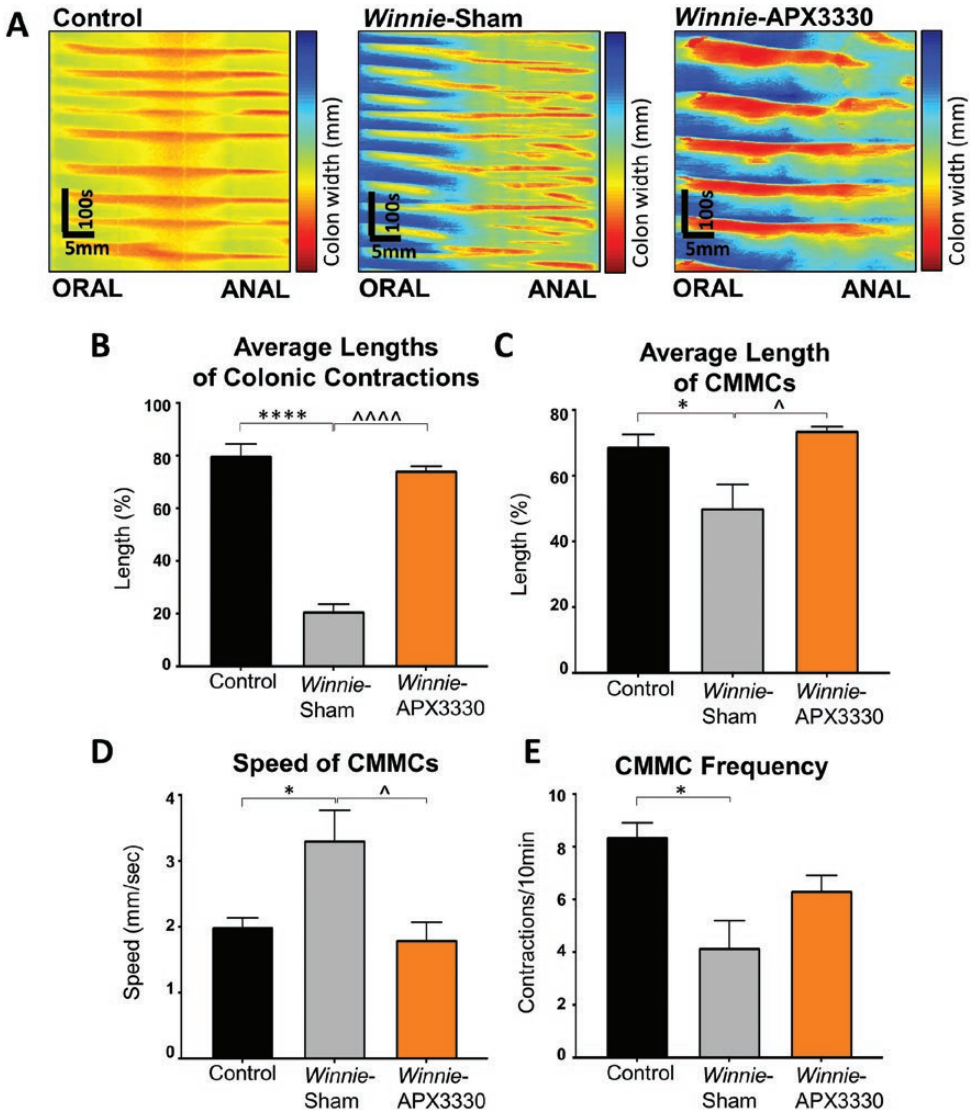

FIGURE 4. The effects of APX3330 treatment on parameters of colonic motility. A, Video recordings from ex vivo whole colon samples were transposed into spatiotemporal maps. Contractions were distinguished as red and relaxation as blue from C57BL/6 control, Winnie sham-treated, and Winnie APX3330-treated mice (n = 6/group). B, Average length of contractions in proportion to the whole colon length C. Average length of colonic migrating motor complexes (CMMCs, white arrows in A) defined as contractions initiated from the oral end that propagated toward the anal end for >50% of the colon length. D, Speed of propagation of CMMCs. E, Frequency of CMMCs quantified as the number of contractions per 10 minutes. Data expressed as mean ± SEM, *$P < 0.05$, ****$P < 0.0001$ compared with C57BL/6 control mice; ^$P < 0.05$, ^^^^$P < 0.0001$ compared with Winnie sham-treated mice.

CMMC speed: 3.3 ± 0.5 mm/sec, $n = 6$) than in C57BL/6 mice (2.0 ± 0.1 mm/sec, $P < 0.05$, $n = 6$). After APX3330 treatment, CMMC speed in *Winnie* mice (1.8 ± 0.3 mm/sec, $n = 6$) was significantly slower than in *Winnie* sham-treated mice ($P < 0.05$) and comparable with the speed of CMMCs in C57BL/6 mice (Fig. 4D). CMMCs in *Winnie* sham-treated mice (4.0 ± 1.0 CMMCs/10 mins, $n = 6$) were significantly less frequent than in C57BL/6 mice (8.0 ± 0.5 CMMCs/10 mins, $P < 0.05$, $n = 6$). Treatment with APX3330 tended to increase the frequency of CMMCs (6.3 ± 1.0 CMMCs/10 mins, $n = 6$) compared with *Winnie* sham-treated mice, but significant difference was not achieved (Fig. 4E).

APX3330 Treatment Alleviated Enteric Neuropathy in *Winnie* Mice

An antibody specific to neuronal microtubule protein β-tubulin (|||) was used to label nerve fibres in cross-sections of the distal colon from C57BL/6 control, *Winnie* sham-treated and *Winnie* APX3330-treated mice (Fig. 5A). *Winnie* sham-treated mice had a significantly lower nerve fibre density in the distal colon (6.7 ± 1.2%, $P < 0.001$, $n = 5$) than C57BL/6 control mice (14.4 ± 1.2%, $n = 5$; Fig. 5A, 5B), while APX3330 treatment improved nerve fibre density in the colon (14.5 ± 0.8, $P < 0.001$, $n = 5$; Fig. 5A, 5B).

Myenteric neurons were identified with a pan neuronal marker anti-MAP2 antibody in LMMP preparations from C57BL/6 control, *Winnie* sham-treated and *Winnie* APX3330-treated mice (Fig. 5A). Fewer myenteric neurons per ganglion were observed in *Winnie* sham-treated mice (20 ± 1 neurons, $n = 5$) than in C57BL/6 control mice (37 ± 4 neurons per ganglion, $P < 0.01$, $n = 5$; Fig. 5A, 5C). The APX3330 treatment alleviated the loss of myenteric neurons in Winnie mice (32 ± 3 neurons per ganglion, $P < 0.05$ compared with Winnie sham-treated group, n = 5; Fig. 5A, 5C). In Winnie sham-treated mice, there were fewer myenteric neurons per unit area (189 ± 17 neurons per mm^2, $n = 5$) than in C57BL/6 control mice (348 ± 36 neurons per mm^2, $P < 0.05$, n = 5; Fig. 5A, 5D). The APX3330 treatment alleviated loss of myenteric neurons (320 ± 34 neurons per mm^2, $P < 0.05$, n = 5) compared with Winnie sham-treated mice (Fig. 5A, 5D).

Glial cell density was identified with an anti-GFAP antibody assessed in the myenteric plexus of the distal colon relative to the ganglion area in LMMP preparations from C57BL/6 control, Winnie sham-treated, and Winnie APX3330-treated mice (Fig. 5A). Winnie sham-treated mice had a significant decrease in glial cell density (15.6 ± 0.6%, $n = 5$) compared with C57BL/6 control mice (26.5 ± 0.9%, $P < 0.01$, n = 5; Fig. 5A, 5E). The APX3330 treatment of Winnie mice improved GFAP density (22.0 ± 0.8%, $P < 0.01$, n = 5) when compared with Winnie sham-treated mice (Fig. 5A, 5E).

APX3330 Treatment Reduced Oxidative Stress and Associated DNA Damage

The fluorescent mitochondrial superoxide marker MitoSOX Red was used to evaluate superoxide production in distal colon myenteric ganglia from C57BL/6 control, Winnie sham-treated, and Winnie APX3330-treated mice (Fig. 6A). High levels of MitoSOX fluorescence were evident in the myenteric plexus of Winnie sham-treated mice (30.9 ± 2.7%, $P < 0.05$, n = 5) when compared with C57BL/6 control mice (16.4 ± 0.4%, n = 5; Fig. 6A, 6B). Increased superoxide production in the myenteric plexus was alleviated in the colons from Winnie APX3330-treated mice (13.8 ± 2.3%, $P < 0.01$, n = 5; Fig. 6A, 6B).

Translocation of HMGB1 protein from nuclei to cytoplasm identifies its conversion to a damage-associated molecular pattern (DAMP) that is released by dying cells to stimulate an immune response.[37] The HMGB1 translocation from neuronal nuclei to cytoplasm was analyzed within LMMP preparations from C57BL/6 control, Winnie sham-treated, and Winnie APX3330-treated mice (Fig. 6A'). In Winnie sham-treated mice, many more cells exhibited HMGB1 translocation into the cytosol (17 ± 3 neurons per ganglion, $P < 0.01$, $n = 5$) than in C57BL/6 control mice (0 ± 0 neuron per ganglion, n = 5; Fig. 6A', 6C). The APX3330 treatment attenuated cytoplasmic translocation of HMGB1 in the myenteric ganglia (1 ± 0 neuron per ganglion, $P < 0.05$, n = 5) compared with Winnie sham-treated mice (Fig. 6A', 6C).

The APE1/Ref-1 expression was determined by immunofluorescence within the myenteric plexus in the colon cross-sections and LMMP preparations from C57BL/6 control, Winnie sham-treated, and Winnie APX3330-treated mice (Fig. 7A, 7 A'). A significant increase in APE1/Ref-1 intensity was observed in the colon cross-sections from Winnie sham-treated mice (32.2 ± 3.3%, $P < 0.0001$, n = 5) compared with C57BL/6 control mice (11.7 ± 0.9%, n = 5; Fig. 7A, 7B). The APX3330 treatment reduced this overexpression of APE1/Ref-1 in colon cross-sections (13.8 ± 1.3%, $P < 0.001$, $n = 5$) compared with Winnie sham-treated mice (Fig. 7A, 7B). The level of APE1/Ref-1 immunoreactivity was increased within the myenteric ganglia of Winnie sham-treated mice (17.4 ± 1.1%, $P < 0.05$, n = 5) compared with C57BL/6 control mice (11.8 ± 1.5%, n = 5; Fig. 7A', 7C). In contrast, immunoreactivity in the myenteric ganglia from Winnie APX3330-treated mice (6.2 ± 1.1%, P < 0.001 compared with Winnie sham-treated group, n = 5) was similar to C57BL/6 controls (Fig. 7A', 7C).

Myenteric neurons were co-immunolabeled with a panneuronal marker, MAP2, and an oxidative DNA damage marker, 8-OHdG (Fig. 8A). Overall, 8-OHdG immunofluorescence density was significantly greater in Winnie sham-treated mice (17.6 ± 1.8%, $P < 0.01$, $n = 5$) than in C57BL/6 control mice (4.6 ± 1.1%, n = 5; Fig. 8A, 8B). This immunoreactivity subsided in Winnie APX3330-treated

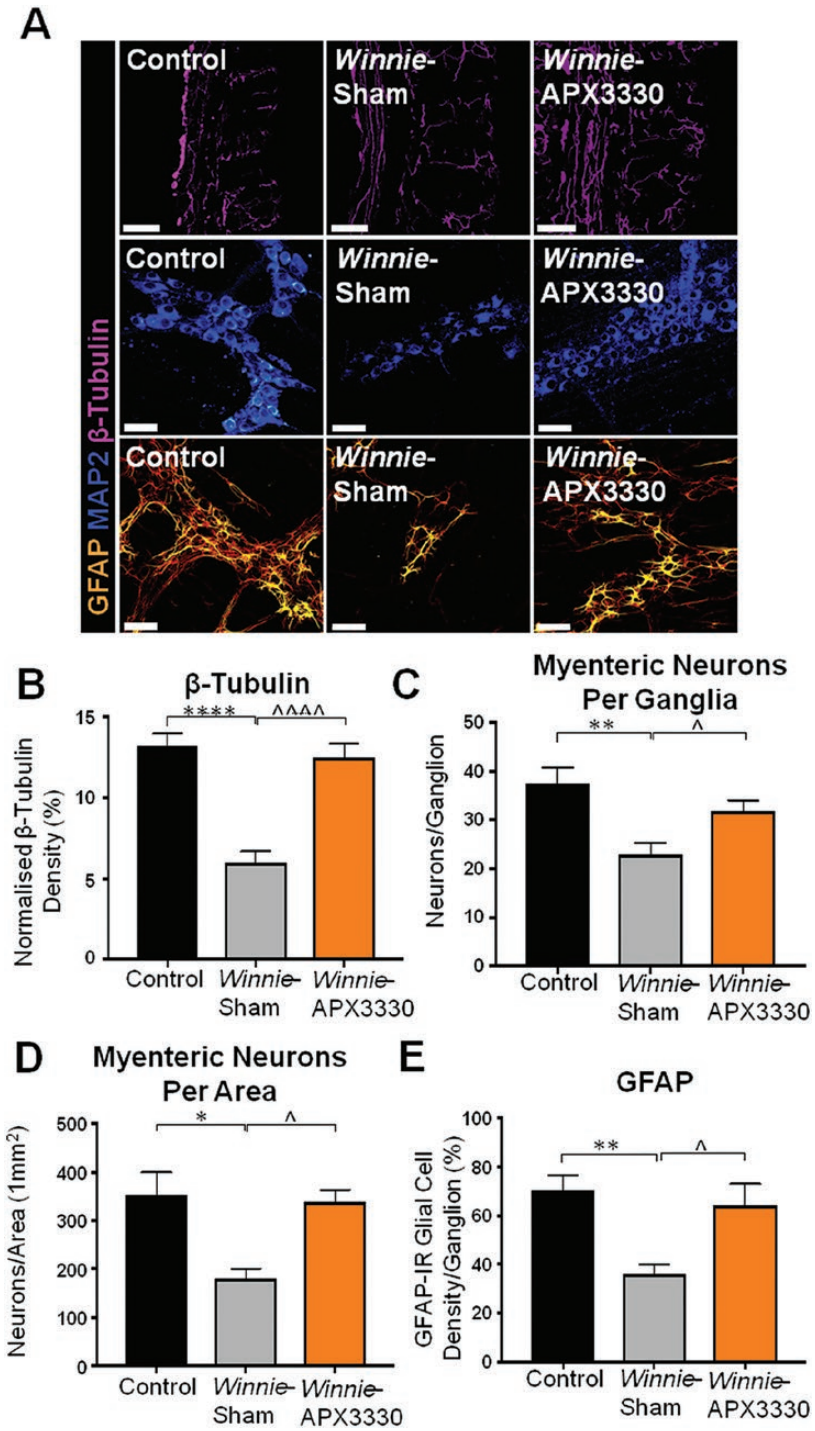

FIGURE 5. THE APX3330 T reatment promoted myenteric neuronal survival and ameliorated nerve fiber and glial cell density in the myenteric plexus in Winnie mice. A, Neuronal microtubule proteins were labeled by immunofluorescence using β-tubulin (III; purple) antibody to identify nerve fibers innervating the colon in cross-sections (scale bar = 100 μm, 20x magnification). Anti-MAP2-IR antibody staining (blue) for myenteric neurons in LMMP preparations (scale bar = 50 μm, x40 magnification). Glial cells were labeled with an anti-GFAP antibody (orange) in the myenteric plexus of the colon from C57BL/6 control, Winnie sham-treated, and Winnie APX3330-treated mice (scale bar = 50 μm, 40x magnification). B, Density of β-tubulin (III)-IR nerve fibers normalized to colon thickness in C57BL/6 control, Winnie sham-treated, and Winnie APX3330-treated mice (n = 5/group). C, Quantitative analysis of myenteric neurons per ganglion C57BL/6 control, Winnie sham-treated, and Winnie APX3330-treated mice (n = 5/group). D, Myenteric neurons were quantified per area in LMMP preparations of C57BL/6 control, Winnie sham-treated, and Winnie APX3330-treated mice (n = 5/group). E, Density of GFAP-IR glial cells per ganglia in C57BL/6 control, Winnie sham-treated, and Winnie APX3330-treated mice (n = 5/group). Data expressed as mean ± SEM, *$P < 0.05$, **$P < 0.01$, ***$P < 0.001$, compared with C57BL/6 control mice; ^$P < 0.05$, ^^$P < 0.01$, ^^^$P < 0.001$ compared with Winnie sham-treated mice.

mice (3.8 ± 1.7%, $P < 0.01$, n = 5) to levels comparable with C57BL/6 control mice (Fig. 8A, 8B). These results were consistent with the number of myenteric neurons colocalized with 8-OHdG, which was significantly larger in Winnie sham-treated mice (26 ± 8.0%, $P < 0.01$, n = 5) than in C57BL/6 control mice (1.2 ± 1.0%, $n = 5$; Fig. 8A, 8C) or in Winnie APX3330-treated mice (1.9 ± 0.8%, $P < 0.01$ compared with Winnie sham-treated group, n = 5; Fig. 8A, 8C).

DISCUSSION

This is the first study to investigate the effects of APX3330, a small molecule inhibitor of APE1/Ref-1 redox signaling, in a clinically relevant animal model of IBD. Our study provides novel findings on the presence of APE1/Ref-1 in enteric neurons, increased level of APE1/Ref-1 in both the mucosa and myenteric ganglia, and significant increase in mitochondrial reactive oxygen species (ROS) production, leading to oxidative DNA damage and translocation of HMGB1 in the colons from Winnie mice. Targeting this pathway with APX3330 ameliorated enteric neuropathy and colonic dysmotility and altered GI transit while providing anti-inflammatory and antioxidant effects in the Winnie murine model of spontaneous chronic colitis. These results demonstrate that APX3330 had prominent therapeutic effects in a preclinical animal model of IBD.

The current treatments for IBD are limited due to inefficacy, intolerance, resistance, side effects, and inability to maintain remission.[38, 39] Front-line treatments tend to involve immunosuppression, which has long-term detrimental effects that lead to diminished quality of life in IBD patients.[40–43] Several new biological treatments have been introduced into clinic that have helped to reduce use of corticosteroids, but many patients stop responding to the clinically approved drugs, so there is still a large unmet need for IBD treatment.[44]

Oxidative stress is a major contributing factor to tissue injury in IBD patients. Reduced mucosal antioxidant capacity and plasma antioxidants have been shown in patients with active CD and UC.[20, 45, 46] However, free radical antioxidants failed in clinical trials, as treatment with general antioxidants does not affect specific signaling and localized oxidative pathways or reversal of DNA damage within cells and subsequently within subcellular elements of cells.[47] Therefore, new therapeutic strategies to block the major sources of oxidative stress are essential. Our study targeted a key molecule involved in oxidative DNA damage/repair mechanisms, APE1/Ref-1, which underpins cellular homeostasis and regulates multiple downstream inflammatory mediators that fuel uncontrolled homeostatic disbalance, causing detrimental effects observed in IBD. APX3330 has the unique ability to suppress inflammation and chemotherapy-induced enhanced redox signaling activity of APE1/Ref-1 while providing neuroprotection in dorsal root ganglion neurons through an increase in oxidative DNA damage repair.[22, 48–50] A recent phase 1 clinical trial of APX3330 in cancer patients demonstrated no significant toxicities/adverse effects, demonstrated disease stabilization in 6 patients, with 4 on drug for an extended time (252, 337, 357, and 421 days), and predicted pharmacokinetics and target engagement (NCT03375086).[51, 52] Here we tested whether APX3330 alleviates intestinal inflammation, GI dysfunction, and damage to enteric neurons in a preclinical model of spontaneous chronic colitis.

Rectal bleeding, prolapse, chronic diarrhea, and lack of body weight gain are clinical symptoms of chronic colitis in the Winnie mouse model.[24–26, 30] Treatment with APX3330 improved clinical signs associated with colonic inflammation in this model of chronic colitis. APX3330 attenuated rectal bleeding, improved stool consistency, and prevented loss of body weight in Winnie mice. Gross morphological damage of the colon demonstrated aberrant crypt architecture, crypt elongation, abscesses, epithelial damage and ulceration in Winnie sham-treated mice. Increased colonic crypt length due to epithelial hyperplasia is consistently observed in Winnie mice with chronic colitis[24–26] and in other models of chronic colitis,[53, 54] although in chemically induced models of colitis (trinitrobenzenesulfonic acid, DSS), both crypt elongation and crypt destruction with mucosal erosion have been reported.[55, 56] These parameters of gross morphological damage were alleviated by APX3330 treatment. High levels of colonic leukocyte infiltration and fecal Lcn-2 are reliable markers of inflammation that are prominent in multiple animal models of experimental colitis in Winnie mice.[26, 31] APX3330 alleviated the immune response in the Winnie mice after a 2-week treatment regimen. This was shown by reduced CD45+ leukocyte infiltration throughout the distal colon and reduced levels of fecal Lcn-2 in Winnie APX3330-treated mice. Further studies need to be performed to define APX3330 effects on specific types of immune cells infiltrating the colon and specific inflammatory mediators.

Winnie mice show an increase in total GI transit time due to a substantial delay in the cecum, although accelerated colonic transit is evident, consistent with previous reports in this model.[31] Similarly, constipation in the proximal colon[57] and accelerated distal colonic transit[58, 59] are common in patients with severe UC. Persistent alterations of GI transit in IBD patients and animal models beyond periods of acute inflammation indicate that damage to the intestinal innervation controlling GI functions is involved.[60] Intrinsic and extrinsic innervations are integral to the functions of the GI tract.[61] Significant changes to intestinal transit result from modulation of the sympathetic and parasympathetic innervation of the GI tract observed in both Winnie and chemically induced models of colitis.[18, 26, 31, 60] In addition to changes in GI transit time, there was a notable decrease in the average length of colonic contractions with a reduction in length, increased speed, and lower frequency of CMMCs demonstrating distorted colonic motor activity in Winnie mice compared with controls. The APX3330 treatment successfully restored total GI and colonic transit time in vivo and colonic CMMC lengths to control levels ex vivo. These

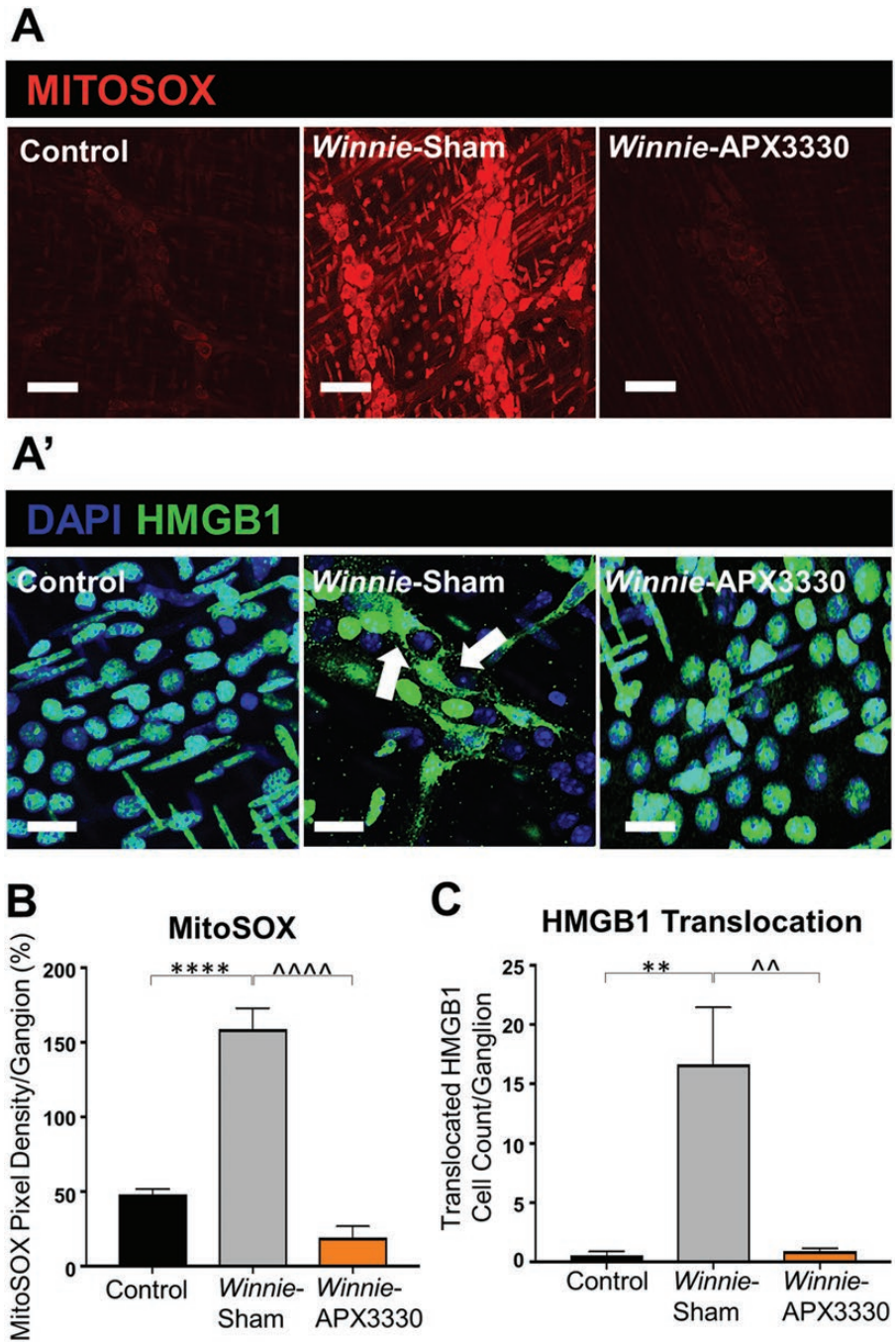

FIGURE 6. Effects of APX3330 treatment on superoxide production and HMGB1 translocation in the myenteric plexus of Winnie mice. A, LMMP preparations of the distal colon were labeled with Mitochondrial superoxide marker MitoSOX (red) indicative of oxidative stress. Increased MitoSOX immunofluorescence was evident in the myenteric ganglia of Winnie sham-treated (n = 5) compared with C57BL/6 control (n = 5) mice (scale bar = 100 µm, 40x magnification). This was alleviated in Winnie APX3330-treated (n = 5) mice (scale bar = 100 µm) (A') HMGB1 immunoreactivity (green) colocalized with nuclei marker DAPI (blue) in the myenteric plexus. Translocation of nuclear HMGB1 to cytosol (marked with white arrows) was observed in Winnie sham-treated compared with C57BL/6 control mice and was averted in Winnie APX3330-treated mice (n = 5/group; scale bar = 50 µm, 60x magnification). B, MitoSOX fluorescence intensity was assessed relative to ganglion area. C, The number of cells with translocation of HMBG1 from nucleus to cytoplasm was quantified in the myenteric ganglia. Data expressed as mean ± SEM, **P* < 0.05, ***P* < 0.01 compared with C57BL/6 control mice; ^*P* < 0.05, ^^*P* < 0.01 compared with Winnie sham-treated mice.

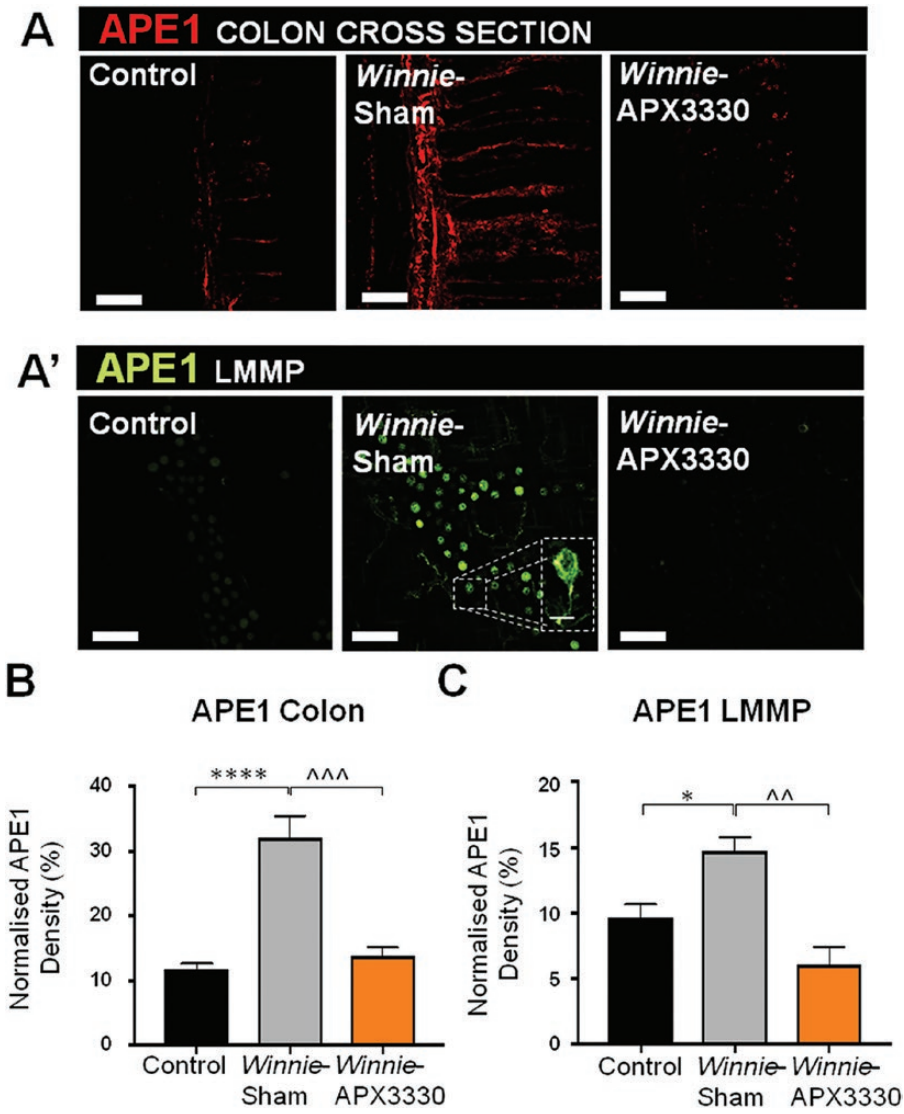

FIGURE 7. The effects of APX3330 treatment on APE1/Ref-1 expression in myenteric neurons of Winnie mice. A, APE1/Ref-1 labeled by immunofluorescence (red) in the colon cross-sections. A', APE1/Ref-1 immunofluorescence (green) in the myenteric plexus in wholemount LMMP preparations. B, Density of APE1/Ref-1 fluorescence in the colon cross-sections relative to the total area of colonic mucosa in C57BL/6, Winnie sham-treated, and Winnie APX3330-treated mice (n = 5/group; scale bar = 100 µm, 20x magnification). C, Density of APE1/Ref-1 fluorescence quantified as a percentage relative to the ganglion area in the myenteric plexus in C57BL/6 control, Winnie sham-treated, and Winnie APX3330-treated mice (n = 5/group; scale bar = 50 µm, 40x magnification). Data expressed as mean ± SEM, *$P < 0.05$, ****$P < 0.0001$ compared with C57BL/6 control mice; ^^^$P < 0.001$ compared with Winnie sham-treated mice.

changes correlate with increased colonic transit time observed in in vivo experiments. Although frequency of CMMCs has not returned to control levels, overall propulsive activities of the colon become more prominent. This positive modulation of the GI motility suggests that APX3330 treatment has direct or indirect effects on intestinal innervation. Though GI transit is influenced by both extrinsic and intrinsic neurons, the ex vivo contractile activity of the isolated colon is driven mainly by enteric neurons within the myenteric ganglia.[62] Accordingly, we focused on the mechanisms underlying these positive effects of APX3330 treatment in the myenteric plexus.

Intestinal inflammation leads to enteric neuropathy, resulting in compromised GI function.[32, 63] The severity of inflammation in the colon has an impact on myenteric neuronal loss in Winnie mice.[26] Loss of myenteric neurons and neuronal fibers occurs in multiple animal models of intestinal inflammation and in IBD patients.[30, 64–68] In addition, reduced expression of GFAP-positive glial cells within myenteric ganglia is seen in Winnie mice in this study. In contrast, studies of colonic biopsies from IBD patients, animal models of colitis, and in vitro cultures yielded divergent results on the expression of GFAP in inflammatory conditions.[69] The

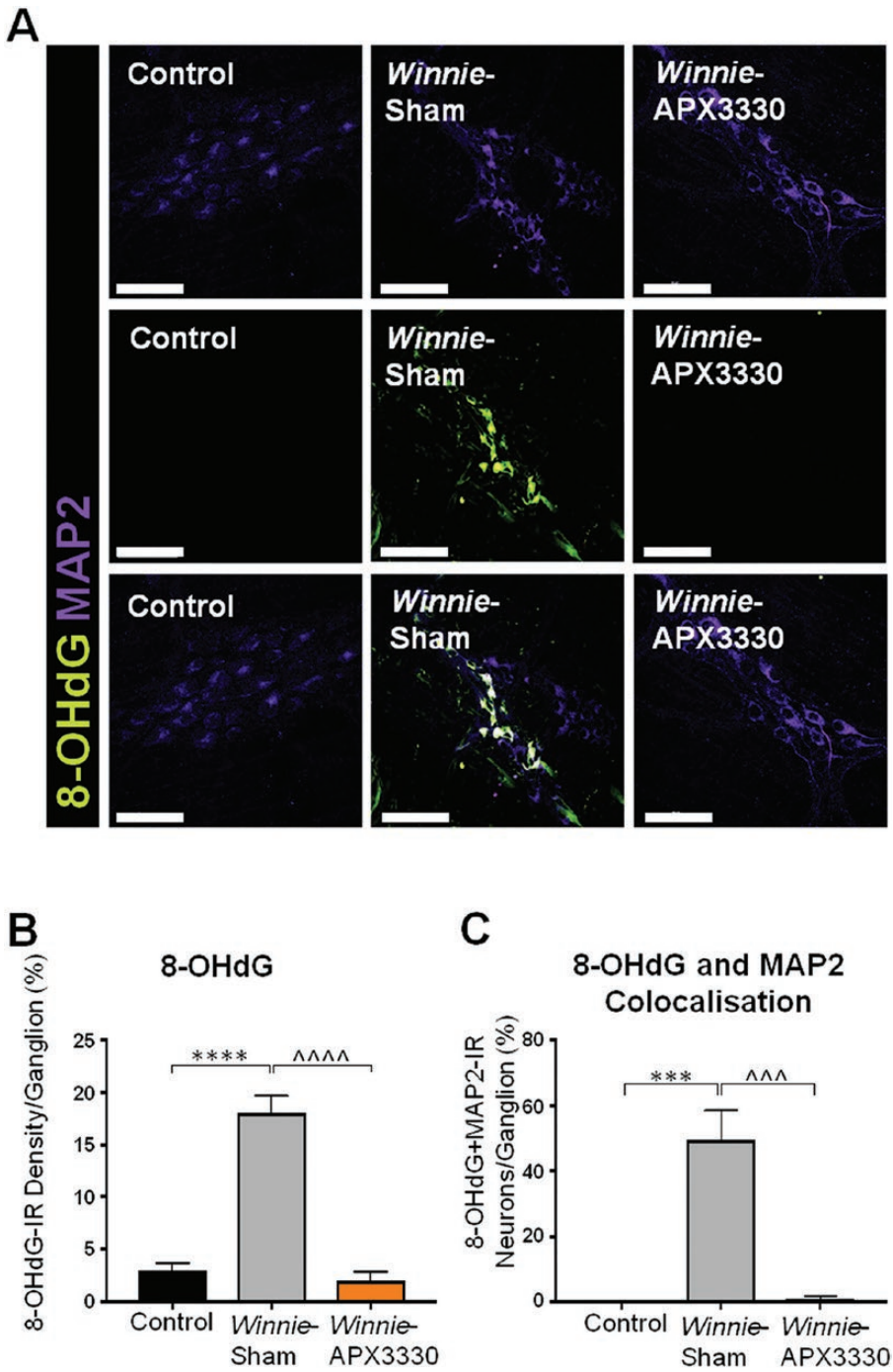

FIGURE 8. The effects of APX3330 treatment on DNA damage in myenteric neurons of Winnie mice. A, DNA damage was observed with an anti-8-OHdG (green) antibody in myenteric neurons immunoreactive for MAP2 (purple; scale bar = 50 µm, 40x magnification). B, The density of 8-OHdG-IR cells was quantified as a percentage relative to the ganglion area within myenteric plexus in C57BL/6 control, Winnie sham-treated, and Winnie APX3330-treated mice (n = 5/group). C, The number of neurons with colocalization of 8-OHdG-IR and MAP2-IR relative to the total number of neurons per ganglion area. Data expressed as mean ± SEM, $^{**}P < 0.01$ compared with C57BL/6 control; $^{\wedge\wedge}P < 0.01$ compared with Winnie sham-treated mice.

reduced immunofluorescence density of GFAP-positive glial cells in our study may be due to either loss of GFAP-positive glial cells, phenotypic changes, or decreased expression of the protein corresponding to a loss of glial reactivity. Other types of glial cells should be considered in future studies of this model. Enteric glial cells regulate intestinal homeostasis

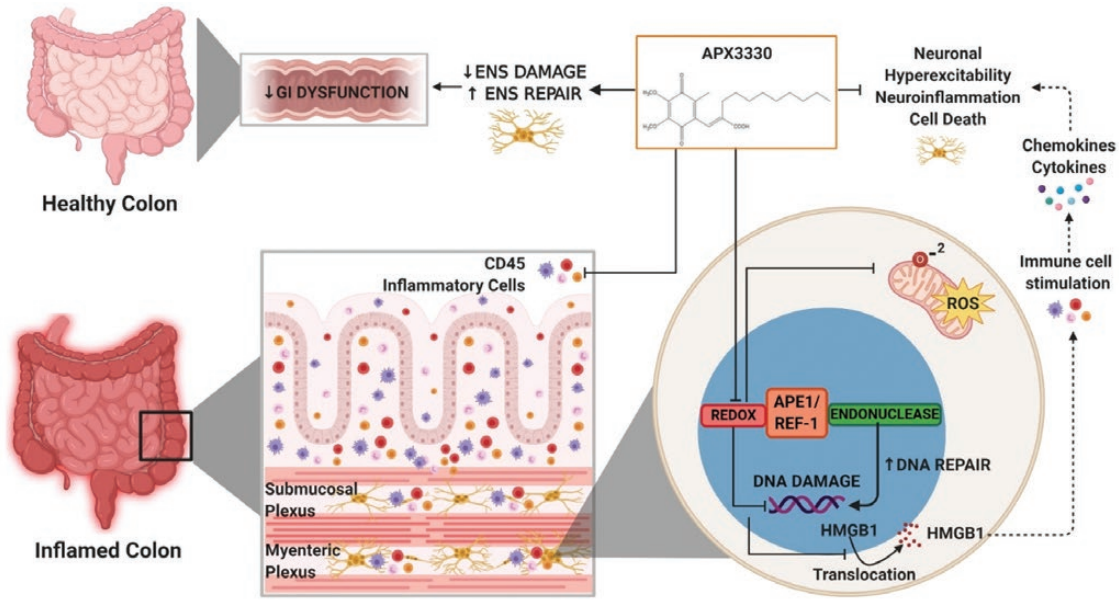

FIGURE 9. Effects of APX3330 treatment on enteric neurons and GI functions. In the inflamed colon, high levels of colonic leukocyte infiltration and fecal Lcn-2 were alleviated by APX3330 treatment. Chronic intestinal inflammation associates with the damage to the enteric nervous system embedded within the intestinal wall and controls gastrointestinal (GI) functions. In enteric neurons, APX3330 treatment APX3330 reduces oxidative stress via inhibition of APE1/Ref-1's redox signaling, mitochondrial superoxide production, and oxidative DNA damage. However, suppressing APE1/Ref-1 redox activity enhances APE1/Ref-1's endonuclease repair activity. DNA damage induces translocation of HMGB1 from the nucleus to the cytoplasm. Acetylated cytosolic HMGB1 released from cells into extracellular space interacts with immune cells and stimulates production of cytokines and chemokines leading to neuroinflammation, hyperexcitability, and neuronal death (dashed line: not studied in our model). After APX3330 treatment, HMGB1 was retained in the nuclei of myenteric neurons. Targeting this pathway with APX3330 ameliorated enteric neuropathy, ameliorated colonic dysmotility, and altered GI transit leading to improved clinical signs associated with chronic colitis (created with BioRender.com).

and protect enteric neurons from oxidative stress–induced death.[70, 71] Loss of GFAP-positive glial cells causes degeneration of enteric neurons and intestinal inflammation.[72, 73] Altered signaling between enteric glia and neurons contributes to colonic dysmotility.[74] However, in inflammatory conditions, activated enteric glial cells mediate neuronal death via activation of purinergic signaling.[75] Purinergic transmission plays an important role in both excitatory and inhibitory neuronal pathways and sensory transduction in the ENS.[76] Purinergic signaling via P2 receptors plays an important role in controlling nuclear maintenance of APE1/Ref-1.[77] Activation of P2 receptors and intracellular ROS production cause APE1/Ref-1 translocation from the nucleus to cytoplasm,[77] which was also observed in our study. The role of purinergic signaling in regulation of APE1/Ref-1 function in various functional types of enteric neurons needs to be further elucidated.

APX3330 treatment alleviated loss of myenteric neurons, improved nerve fiber, and GFAP immunoreactivity in the myenteric ganglia when compared with Winnie sham-treated mice. APX3330 has been proven to be neuroprotective in sensory neurons after insults caused by ionizing radiation, cheotherapeutic agents, and inflammatory stimuli all producing oxidative DNA damage acted upon by APE1/Ref-1.[14, 22, 50, 78, 79] These studies showed that enhancement of the DNA repair function of APE1/Ref-1—but not its redox signaling—underlies neuroprotective effects of APX3330 in sensory neurons. This was demonstrated using both a genetic and small molecule approach with APX3330.[14, 48, 50, 78] Facilitation of the endonuclease activity of APE1/Ref-1 stimulates base excision repair (BER) of oxidative DNA damage in neurons.[14] Our study provides novel findings on the presence of APE1/Ref-1 in enteric neurons and increased level of APE1/Ref-1 in both the mucosa and myenteric ganglia in the colons from Winnie mice. These results are consistent with findings in the colon tissues removed from IBD patients with active inflammation[19] and in the colonic epithelium of an animal model of DSS-induced colitis.[21] Inflammation caused by pathogenic bacteria, ionizing radiation, ROS, and toxic agents transiently increase intracellular APE1/Ref-1 in gastric epithelial cells and sensory neurons.[79, 80] Our results indicate that APX3330 treatment alleviates the APE1/Ref-1 redox activity in Winnie mice after the 2-week treatment regimen. As APX3330 regulates the inflammatory response, loss of enteric neurons, and immunoreactivity of GFAP in our model of IBD, we tested if these effects result from dysregulation of ROS production in the myenteric plexus.

In the GI tract, the main sources of ROS are the nicotinamide adenine dinucleotide phosphate (NADPH), oxidase

enzymes (NOX and dual oxidase [DUOX]), NOS and the mitochondrial electron transport chain (mETC). Both NOX and DUOX produce ROS not as a by-product but as a primary function. Gastrointestinal tissues express multiple NOX isoforms, including NOX1, NOX2, NOX4, and DUOX2 within different cell types including macrophages, lymphocytes and neutrophils, epithelial cells, fibroblasts, and glandular cells throughout the GI tract.[81] A recent study demonstrated that enteric glial cells increase expression of NOX-2 in response to inflammatory stimuli.[82] The NOX expression in enteric neurons of the GI tract has not been investigated. It is known that mitochondria can regulate, activate, differentiate, and aid survival of immune cells.[83] Deregulation of the mitochondrial electron transport chain, with increased mitochondrial ROS (mtROS) levels, was observed in IBD patients.[84] Oxidants produced by GI cells provide an antibacterial defence.[85] Uncontrolled and persistent overproduction of ROS due to upregulation of oxidases or altered mitochondrial function and/or inadequate removal of ROS by antioxidant systems causes tissue injury and exacerbates inflammation, eventually leading to other chronic complications such as fibrosis, neoplasia, and extraintestinal symptoms.[47, 86] In addition, it has been shown that the production of ROS induces DNA damage leading to neuronal loss.[87] In our study, oxidative stress in myenteric neurons and surrounding cells was shown by the increased mitochondrial superoxide production in Winnie mice. Myenteric neurons in Winnie mice exhibit increased mitochondrial superoxide and oxidative stress–induced DNA damage, as seen in multiple studies that describe increase in oxidative DNA damage in the colonic mucosa of IBD patients[9, 20, 88] and chemically induced colitis.[21] Our results demonstrate that APX3330 reduced oxidative stress via its redox inhibition of APE1/Ref-1 and oxidative DNA damage in chronic colitis. On the other hand, suppressing APE1/Ref-1's redox activity with APX3330 enhances APE1/Ref-1's endonuclease repair activity via the BER pathway, which takes place in both the nuclei and mitochondria. The APE1/Ref-1's endonuclease activity is responsible for repairing DNA damage induced by oxidative stress, alkylating agents, and ionizing radiation.[11, 89] Further studies are required to elucidate APE1/Ref-1's endonuclease repair activity in enteric neurons after APX3330 treatment.

DNA damage can induce translocation of HMGB1 from the nucleus to the cytoplasm.[90–92] Significantly higher numbers of cells in the myenteric plexus of Winnie mice displayed translocation of HMGB1 from the nucleus to the cytoplasm, indicating cellular stress. High mobility group box 1 protein has various functions that depend on its location outside or inside the cell. Acetylated cytosolic HMGB1 released from cells into extracellular space acts as a proinflammatory mediator interacting with immune cells and stimulating production of cytokines and chemokines,[37, 93] leading to neuroinflammation, hyperexcitability, and neuronal death.[94, 95] APE1/Ref-1 regulates the release of cytosolic HMGB1 and the inflammatory signaling to extracellular HMGB1.[96] After APX3330 treatment, HMGB1 was retained in the nuclei of myenteric neurons, thereby reducing release of HMGB1 and presumably increasing survival of colonic myenteric neurons in Winnie mice. This is consistent with findings that nuclear HMGB1 directly interacts with and enhances the endonuclease activity of APE1/Ref-1,[97] acting as a cofactor modulating BER capacity in cells.[98]

CONCLUSION

This study is the first to provide evidence for therapeutic effects of APX3330 in alleviating inflammatory responses, disease severity, GI dysfunction, and enteric neuropathy. Inhibition of mitochondrial superoxide production, APE1/Ref-1 redox signaling, oxidative DNA damage, and translocation of HMGB1 are some of the mechanisms involved in neuroprotective effects of APX3330 in enteric neurons (Fig. 9). Further studies are needed to elucidate more detailed molecular mechanisms underlying the role of APE1/Ref-1, its redox signaling, and DNA damage/repair functions in enteric neurons, in addition to long-term effects of APX3330 treatment. However, results of the recent clinical trial in oncology patients with advanced solid tumors demonstrated that long-term treatment with APX3330 did not show any safety concerns.[51, 52] Thus, specific inhibition of the redox signaling function of the APE1/Ref-1 molecule is a novel strategy that might lead to a possible application of APX3330 for the treatment of IBD with good tolerability.

REFERENCES

1. Burisch J, Munkholm P. The epidemiology of inflammatory bowel disease. *Scand J Gastroenterol.* 2015;50:942–951.
2. Chang CW, Wong JM, Tung CC, et al. Intestinal stricture in Crohn's disease. *Intest Res.* 2015;13:19–26.
3. de Jonge WJ. The Gut's little brain in control of intestinal immunity. *ISRN Gastroenterol.* 2013;2013:630159.
4. Lakhan SE, Kirchgessner A, Neuroinflammation in inflammatory bowel disease. *J Neuroinflammation.* 2010;7:37.
5. Lomax AE, Fernández E, Sharkey KA. Plasticity of the enteric nervous system during intestinal inflammation. *Neurogastroenterol Motil.* 2005;17:4–15.
6. Knowles CH, Lindberg G, Panza E, et al. New perspectives in the diagnosis and management of enteric neuropathies. *Nat Rev Gastroenterol Hepatol.* 2013;10:206–218.
7. Brown IAM, Gulbransen BD. The antioxidant glutathione protects against enteric neuron death in situ, but its depletion is protective during colitis. *Am J Physiol Gastrointest Liver Physiol.* 2018;314:G39–G52.
8. Bagyánszki M, Bódi N. Diabetes-related alterations in the enteric nervous system and its microenvironment. *World J Diabetes.* 2012;3:80–93.
9. D'Incà R, Cardin R, Benazzato L, et al. Oxidative DNA damage in the mucosa of ulcerative colitis increases with disease duration and dysplasia. *Inflamm Bowel Dis.* 2006;10:23–27.
10. Keshavarzian A, Banan A, Farhadi A, et al. Increases in free radicals and cytoskeletal protein oxidation and nitration in the colon of patients with inflammatory bowel disease. *Gut.* 2003;52:720–728.
11. Shah F, Logsdon D, Messmann RA, et al. Exploiting the Ref-1-APE1 node in cancer signaling and other diseases: from bench to clinic. *NPJ Precis Oncol.* 2017;1:19.
12. Tell G, Quadrifoglio F, Tiribelli C, et al. The many functions of APE1/Ref-1: not only a DNA repair enzyme. *Antioxid Redox Signal.* 2009;11:601–620.
13. Kelley MR, Georgiadis MM, Fishel ML. APE1/Ref-1 role in redox signaling: translational applications of targeting the redox function of the DNA repair/redox protein APE1/Ref-1. *Curr Mol Pharmacol.* 2012;5:36–53.

14. Kelley MR, Jiang Y, Guo C, et al. Role of the DNA base excision repair protein, APE1 in cisplatin, oxaliplatin, or carboplatin induced sensory neuropathy. *Plos One.* 2014;9:e106485.
15. Fishel ML, He Y, Reed AM, et al. Knockdown of the DNA repair and redox signaling protein Ape1/Ref-1 blocks ovarian cancer cell and tumor growth. *DNA Repair (Amst).* 2008;7:177–186.
16. Luo M, Delaplane S, Jiang A, et al. Role of the multifunctional DNA repair and redox signaling protein Ape1/Ref-1 in cancer and endothelial cells: small-molecule inhibition of the redox function of Ape1. *Antioxid Redox Signal.* 2008;10:1853–1867.
17. Vascotto C, Fantini D, Romanello M, et al. APE1/Ref-1 interacts with NPM1 within nucleoli and plays a role in the rRNA quality control process. *Mol Cell Biol.* 2009;29:1834–1854.
18. Liu H, Liu X, Zhang C, et al. Redox imbalance in the development of colorectal cancer. *J Cancer.* 2017;8:1586–1597.
19. Hofseth LJ, Khan MA, Ambrose M, et al. The adaptive imbalance in base excision–repair enzymes generates microsatellite instability in chronic inflammation. *J Clin Invest.* 2003;112:1887–1894.
20. Lih-Brody L, Powell SR, Collier KP, et al. Increased oxidative stress and decreased antioxidant defenses in mucosa of inflammatory bowel disease. *Dig Dis Sci.* 1996;41:2078–2086.
21. Chang IY, Kim JN, Maeng YH, et al. Apurinic/apyrimidinic endonuclease 1, the sensitive marker for DNA deterioration in dextran sulfate sodium-induced acute colitis. *Redox Rep.* 2013;18:165–173.
22. Fehrenbacher JC, Guo C, Kelley MR, et al. DNA damage mediates changes in neuronal sensitivity induced by the inflammatory mediators, MCP-1 and LPS, and can be reversed by enhancing the DNA repair function of APE1. *Neuroscience.* 2017;366:23–35.
23. Kelley MR, Fehrenbacher JC. Challenges and opportunities identifying therapeutic targets for chemotherapy-induced peripheral neuropathy resulting from oxidative DNA damage. *Neural Regen Res.* 2017;12:72–74.
24. Eri RD, Adams RJ, Tran TV, et al. An intestinal epithelial defect conferring ER stress results in inflammation involving both innate and adaptive immunity. *Mucosal Immunol.* 2011;4:354–364.
25. Heazlewood CK, Cook MC, Eri R, et al. Aberrant mucin assembly in mice causes endoplasmic reticulum stress and spontaneous inflammation resembling ulcerative colitis. *PLos Med.* 2008;5:e54.
26. Rahman AA, Robinson AM, Jovanovska V, et al. Alterations in the distal colon innervation in Winnie mouse model of spontaneous chronic colitis. *Cell Tissue Res.* 2015;362:497–512.
27. Robinson AM, Gondalia SV, Karpe AV, et al. Fecal microbiota and metabolome in a mouse model of spontaneous chronic colitis: relevance to human inflammatory bowel disease. *Inflamm Bowel Dis.* 2016;22:2767–2787.
28. Fishel ML, Xia H, McGeown J, et al. Anti-tumor activity and mechanistic characterization of APE1/Ref-1 inhibitors in bladder cancer. *Mol Cancer Ther.* 2019;18:1947–1960.
29. Yang X, Peng Y, Jiang X, et al. The regulatory role of APE1 in epithelial-to-mesenchymal transition and in determining EGFR-TKI responsiveness in non-small-cell lung cancer. *Cancer Med.* 2018;7:4406–4419.
30. Rahman AA, Robinson AM, Brookes SJH, et al. Rectal prolapse in Winnie mice with spontaneous chronic colitis: changes in intrinsic and extrinsic innervation of the rectum. *Cell Tissue Res.* 2016;366:285–299.
31. Robinson AM, Rahman AA, Carbone SE, et al. Alterations of colonic function in the Winnie mouse model of spontaneous chronic colitis. *Am J Physiol Gastrointest Liver Physiol.* 2017;312:G85–G102.
32. Mawe GM. Colitis-induced neuroplasticity disrupts motility in the inflamed and post-inflamed colon. *J Clin Invest.* 2015;125:949–955.
33. Swaminathan M, Hill-Yardin E, Ellis M, et al. Video imaging and spatiotemporal maps to analyze gastrointestinal motility in mice. *J Vis Exp.* 2016:e53828. doi: 10.3791/53828.
34. Curtis MJ, Bond RA, Spina D, et al. Experimental design and analysis and their reporting: new guidance for publication in BJP. *Br J Pharmacol.* 2015;172:3461–3471.
35. Chassaing B, Srinivasan G, Delgado MA, et al. Fecal lipocalin 2, a sensitive and broadly dynamic non-invasive biomarker for intestinal inflammation. *Plos One.* 2012;7:e44328.
36. Roberts RR, Bornstein JC, Bergner AJ, et al. Disturbances of colonic motility in mouse models of Hirschsprung's disease. *Am J Physiol Gastrointest Liver Physiol.* 2008;294:G996–G1008.
37. Paudel YN, Shaikh MF, Chakraborti A, et al. HMGB1: a common biomarker and potential target for TBI, neuroinflammation, epilepsy, and cognitive dysfunction. *Front Neurosci.* 2018;12:628.
38. Ghadir MR, Bagheri M, Vahedi H, et al. Nonadherence to medication in inflammatory bowel disease: rate and reasons. *Middle East J Dig Dis.* 2016;8:116–121.
39. Nitzan O, Elias M, Peretz A, et al. Role of antibiotics for treatment of inflammatory bowel disease. *World J Gastroenterol.* 2016;22:1078–1087.
40. Abegunde AT, Muhammad BH, Ali T. Preventive health measures in inflammatory bowel disease. *World J Gastroenterol.* 2016;22:7625–7644.
41. Gionchetti P, Rizzello F, Annese V, et al.; Italian Group for the Study of Inflammatory Bowel Disease (IG-IBD). Use of corticosteroids and immunosuppressive drugs in inflammatory bowel disease: clinical practice guidelines of the Italian Group for the Study of Inflammatory Bowel Disease. *Dig Liver Dis.* 2017;49:604–617.
42. Hanauer SB. Oral or topical 5-ASA in ulcerative colitis. *Dig Dis.* 2016;34:122–124.
43. Harris RC. COX-2 and the kidney. *J Cardiovasc Pharmacol.* 2006;47(Suppl 1):S37–S42.
44. Neurath MF. Current and emerging therapeutic targets for IBD. *Nat Rev Gastroenterol Hepatol.* 2017;14:269–278.
45. Achitei D, Ciobica A, Balan G, et al. Different profile of peripheral antioxidant enzymes and lipid peroxidation in active and nonactive inflammatory bowel disease patients. *Dig Dis Sci.* 2013;58:1244–1249.
46. Ishihara T, Tanaka K, Tasaka Y, et al. Therapeutic effect of lecithinized superoxide dismutase against colitis. *J Pharmacol Exp Ther.* 2009;328:152–164.
47. Aviello G, Knaus UG. ROS in gastrointestinal inflammation: rescue or sabotage? *Br J Pharmacol.* 2017;174:1704–1718.
48. Kelley MR, Wikel JH, Guo C, et al. Identification and characterization of new chemical entities targeting apurinic/apyrimidinic endonuclease 1 for the prevention of chemotherapy-induced peripheral neuropathy. *J Pharmacol Exp Ther.* 2016;359:300–309.
49. Kim ER, Chang DK. Colorectal cancer in inflammatory bowel disease: the risk, pathogenesis, prevention and diagnosis. *World J Gastroenterol.* 2014;20:9872–9881.
50. Kim HS, Guo C, Thompson EL, et al. APE1, the DNA base excision repair protein, regulates the removal of platinum adducts in sensory neuronal cultures by NER. *Mutat Res.* 2015;779:96–104.
51. Chu L, Anderson AKL, Landers MA, et al. CTC enumeration and characterization as a pharmacodynamic marker in the phase I clinical study of APX3330, an APE1/Ref-1 inhibitor, in patients with advanced solid tumors. *J Clin Oncol.* 2019;37(15_suppl):e14531.
52. Shahda S, Lakhani NJ, O'Neil B, et al. A phase I study of the APE1 protein inhibitor APX3330 in patients with advanced solid tumors. *J Clin Oncol.* 2019;37(15_suppl):3097.
53. Erben U, Loddenkemper C, Doerfel K, et al. A guide to histomorphological evaluation of intestinal inflammation in mouse models. *Int J Clin Exp Pathol.* 2014;7:4557–4576.
54. Prattis S, Jurjus A, Spontaneous and transgenic rodent models of inflammatory bowel disease. *Lab Anim Res.* 2015;31:47–68.
55. Fuss IJ, Boirivant M, Lacy B, et al. The interrelated roles of TGF-beta and IL-10 in the regulation of experimental colitis. *J Immunol.* 2002;168:900–908.
56. Jiminez JA, Uwiera TC, Douglas Inglis G, et al. Animal models to study acute and chronic intestinal inflammation in mammals. *Gut Pathog.* 2015;7:29.
57. James SL, van Langenberg DR, Taylor KM, et al. Characterization of ulcerative colitis-associated constipation syndrome (proximal constipation). *JGH Open.* 2018;2:217–222.
58. Haase AM, Gregersen T, Christensen LA, et al. Regional gastrointestinal transit times in severe ulcerative colitis. *Neurogastroenterol Motil.* 2016;28:217–224.
59. Rao SS, Read NW, Brown C, et al. Studies on the mechanism of bowel disturbance in ulcerative colitis. *Gastroenterology.* 1987;93:934–940.
60. McQuade RM, Carbone SE, Stojanovska V, et al. Role of oxidative stress in oxaliplatin-induced enteric neuropathy and colonic dysmotility in mice. *Br J Pharmacol.* 2016;173:3502–3521.
61. Uesaka T, Young HM, Pachnis V, et al. Development of the intrinsic and extrinsic innervation of the gut. *Dev Biol.* 2016;417:158–167.
62. Roberts RR, Murphy JF, Young HM, et al. Development of colonic motility in the neonatal mouse-studies using spatiotemporal maps. *Am J Physiol Gastrointest Liver Physiol.* 2007;292:G930–G938.
63. Moynes DM, Lucas GH, Beyak MJ, et al. Effects of inflammation on the innervation of the colon. *Toxicol Pathol.* 2014a;42:111–117.
64. Bernardini N, Segnani C, Ippolito C, et al. Immunohistochemical analysis of myenteric ganglia and interstitial cells of Cajal in ulcerative colitis. *J Cell Mol Med.* 2012;16:318–327.
65. Boyer L, Ghoreishi M, Templeman V, et al. Myenteric plexus injury and apoptosis in experimental colitis. *Auton Neurosci.* 2005;117:41–53.
66. Linden DR, Couvrette JM, Ciolino A, et al. Indiscriminate loss of myenteric neurones in the TNBS-inflamed guinea-pig distal colon. *Neurogastroenterol Motil.* 2005;17:751–760.
67. Nurgali K, Nguyen TV, Matsuyama H, et al. Phenotypic changes of morphologically identified guinea-pig myenteric neurons following intestinal inflammation. *J Physiol.* 2007;583:593–609.
68. Nurgali K, Qu Z, Hunne B, et al. Morphological and functional changes in guinea-pig neurons projecting to the ileal mucosa at early stages after inflammatory damage. *J Physiol.* 2011;589:325–339.
69. Pochard C, Coquenlorge S, Freyssinet M, et al. The multiple faces of inflammatory enteric glial cells: is Crohn's disease a gliopathy? *Am J Physiol Gastrointest Liver Physiol.* 2018;315:G1–G11.

70. Abdo H, Derkinderen P, Gomes P, et al. Enteric glial cells protect neurons from oxidative stress in part via reduced glutathione. *FASEB J.* 2010;24:1082–1094.
71. Roberts JA, Durnin L, Sharkey KA, et al. Oxidative stress disrupts purinergic neuromuscular transmission in the inflamed colon. *J Physiol.* 2013;591:3725–3737.
72. Bush TG, Savidge TC, Freeman TC, et al. Fulminant jejuno-ileitis following ablation of enteric glia in adult transgenic mice. *Cell.* 1998;93:189–201.
73. Cornet A, Savidge TC, Cabarrocas J. Enterocolitis induced by autoimmune targeting of enteric glial cells: a possible mechanism in Crohn's disease? *Proc Natl Acad Sci USA.* 2001;98:13306–13311.
74. McClain JL, Grubišić V, Fried D. Ca2+ responses in enteric glia are mediated by connexin-43 hemichannels and modulate colonic transit in mice. *Gastroenterology.* 2014;146:497–507.e1.
75. Brown IA, McClain JL, Watson RE, et al. Enteric glia mediate neuron death in colitis through purinergic pathways that require connexin-43 and nitric oxide. *Cell Mol Gastroenterol Hepatol.* 2016;2:77–91.
76. Bornstein JC. Purinergic mechanisms in the control of gastrointestinal motility. *Purinergic Signal.* 2008;4:197–212.
77. Pines A, Perrone L, Bivi N, et al. Activation of APE1/Ref-1 is dependent on reactive oxygen species generated after purinergic receptor stimulation by ATP. *Nucleic Acids Res.* 2005;33:4379–4394.
78. Jiang Y, Guo C, Fishel ML, et al. Role of APE1 in differentiated neuroblastoma SH-SY5Y cells in response to oxidative stress: use of APE1 small molecule inhibitors to delineate APE1 functions. *DNA Repair (Amst).* 2009;8:1273–1282.
79. Vasko MR, Guo C, Thompson EL, et al. The repair function of the multifunctional DNA repair/redox protein APE1 is neuroprotective after ionizing radiation. *DNA Repair (Amst).* 2011;10:942–952.
80. O'Hara AM, Bhattacharyya A, Mifflin RC, et al. Interleukin-8 induction by helicobacter pylori; in gastric epithelial cells is dependent on apurinic/apyrimidinic endonuclease-1/redox factor-1. *J Immunol.* 2006;177:7990.
81. Lam G, Apostolopoulos V, Zulli A, et al. NADPH oxidases and inflammatory bowel disease. *Curr Med Chem.* 2015;22:2100–2109.
82. Kimono D, Sarkar S, Albadrani M, et al. Dysbiosis-associated enteric glial cell immune-activation and redox imbalance modulate tight junction protein expression in gulf war illness pathology. *Front Physiol.* 2019;10:1229.
83. Angajala A, Lim S, Phillips JB, et al. Diverse roles of mitochondria in immune responses: novel insights into immuno-metabolism. *Front Immunol.* 2018;9:1605.
84. Dashdorj A, Jyothi KR, Lim S, et al. Mitochondria-targeted antioxidant MitoQ ameliorates experimental mouse colitis by suppressing NLRP3 inflammasome-mediated inflammatory cytokines. *BMC Med.* 2013;11:178.
85. Wink DA, Hines HB, Cheng RY, et al. Nitric oxide and redox mechanisms in the immune response. *J Leukoc Biol.* 2011;89:873–891.
86. Rezaie A, Parker RD, Abdollahi M. Oxidative stress and pathogenesis of inflammatory bowel disease: an epiphenomenon or the cause? *Dig Dis Sci.* 2007;52:2015–2021.
87. Harrison JF, Hollensworth SB, Spitz DR, et al. Oxidative stress-induced apoptosis in neurons correlates with mitochondrial DNA base excision repair pathway imbalance. *Nucleic Acids Res.* 2005;33:4660–4671.
88. Dincer Y, Erzin Y, Himmetoglu S, et al. Oxidative DNA damage and antioxidant activity in patients with inflammatory bowel disease. *Dig Dis Sci.* 2007;52:1636–1641.
89. Krokan HE, Bjørås M. Base excision repair. *Cold Spring Harb Perspect Biol.* 2013;5:a012583.
90. Park JS, Svetkauskaite D, He Q, et al. Involvement of toll-like receptors 2 and 4 in cellular activation by high mobility group box 1 protein. *J Biol Chem.* 2004;279:7370–7377.
91. Tang Y, Zhao X, Antoine D, et al. Regulation of posttranslational modifications of HMGB1 during immune responses. *Antioxid Redox Signal.* 2016;24:620–634.
92. Tsung A, Klune JR, Zhang X, et al. HMGB1 release induced by liver ischemia involves Toll-like receptor 4 dependent reactive oxygen species production and calcium-mediated signaling. *J Exp Med.* 2007;204:2913–2923.
93. Janko C, Filipović M, Munoz LE, et al. Redox modulation of HMGB1-related signaling. *Antioxid Redox Signal.* 2014;20:1075–1085.
94. Kaneko Y, Pappas C, Malapira T, et al. Extracellular HMGB1 modulates glutamate metabolism associated with kainic acid-induced epilepsy-like hyperactivity in primary rat neural cells. *Cell Physiol Biochem.* 2017;41:947–959.
95. Okuma Y, Liu K, Wake H, et al. Anti-high mobility group box-1 antibody therapy for traumatic brain injury. *Ann Neurol.* 2012;72:373–384.
96. Yuk JM, Yang CS, Shin DM, et al. A dual regulatory role of apurinic/apyrimidinic endonuclease 1/redox factor-1 in HMGB1-induced inflammatory responses. *Antioxid Redox Signal.* 2009;11:575–588.
97. Balliano A, Hao F, Njeri C, et al. HMGB1 stimulates activity of polymerase β on nucleosome substrates. *Biochemistry.* 2017;56:647–656.
98. Prasad R, Liu Y, Deterding LJ, et al. HMGB1 is a cofactor in mammalian base excision repair. *Mol Cell.* 2007;27:829–841.